buildings

MDPI

Article

Fatigue Damage Mitigation for Welded Beam-to-Column Connections in Steel High-Rise Buildings Using Passive Vibration Control

Zhao Fang [1], Jianshao Zhang [2,3], Fan Yang [3] and Aiqun Li [3,4,*]

1 School of Architecture Engineering, Nanjing Institute of Technology, Nanjing 211167, China
2 Guang Dong Architectural Design & Research Institute Co., Ltd., Guangzhou 510010, China
3 School of Civil Engineering, Southeast University, Nanjing 210096, China
4 Beijing Advanced Innovation Center for Future Urban Design, Beijing University of Civil Engineering and Architecture, Beijing 100044, China
* Correspondence: aiqunli@seu.edu.cn

Abstract: To investigate the use of vibration control systems in fatigue damage mitigation for welded beam-to-column connections in steel high-rise buildings, cases of both a single connection under constant amplitude cyclic loading and multi-connections in a high-rise building under the stochastic wind, with and without the fluid viscous damper (VFD) and the tuned mass damper (TMD), are discussed respectively. The finite element analysis and the fatigue assessment are conducted so that the mitigation effect, the effect of technical parameters and the conditions of both high-cycle fatigue and low-cycle fatigue are all discussed. The results show that the VFD and the TMD systems are both effective in the mitigation of local fatigue damage along with the structural displacement for both cases. The VFD generally has a better mitigation effect than the TMD and it starts to take effect instantly with the external loading, but it causes a phase difference in structural responses, while the situation of the TMD is quite the opposite. The displacement and the local stress show similar and synchronous mitigation trends so that the damping systems can be designed based on either of them. The VFD should be designed with a smaller damping exponent and a larger damping coefficient in a braced installation form, while the TMD can be designed using the optimal parameters. The optimized VFD layout plan is that VFDs are placed between the two connections with large relative displacement and relative velocity on higher floors and these two connections with VFDs should be near to the targeted connection. The negative fatigue damage mitigation mainly stems from insufficient lateral support force so that the direct installation of VFDs may result in a negative fatigue damage mitigation effect in the connections with limited lateral support.

Keywords: fatigue damage mitigation; fluid viscous damper; tuned mass damper; welded beam-to-column connection; steel high-rise building

Citation: Fang, Z.; Zhang, J.; Yang, F.; Li, A. Fatigue Damage Mitigation for Welded Beam-to-Column Connections in Steel High-Rise Buildings Using Passive Vibration Control. *Buildings* **2022**, *12*, 1898. https://doi.org/10.3390/buildings12111898

Academic Editors: Liqiang Jiang, Jihong Ye and Wei Guo

Received: 7 September 2022
Accepted: 3 November 2022
Published: 5 November 2022

1. Introduction

Welded beam-to-column connections in steel high-rise buildings are susceptible to fatigue damage under cyclic loading, in the form of high-cycle fatigue damage under wind and low-cycle fatigue damage under strong earthquakes. The fatigue damage may even lead to the collapse of the whole building [1]. Under such circumstances, it is indispensable to think of ways to decrease fatigue damage under wind and earthquakes during the design of welded connections. Traditionally, engineers tend to do it by increasing the fatigue damage resistance, but the disadvantages are obvious, in that the increase in the resistance may lead to high costs and a reduction in the structural ductility. Thus, the use of passive vibration control becomes another alternative.

The passive vibration control technique is mainly classified into three types: vibration isolation, energy dissipation and vibration absorbers. Vibration isolation is typically placed

at the foundation of a structure and partially absorbs external input energy before this energy can be transmitted to the structure; therefore, it is limited to the case of a structure under earthquakes and not much applicable to a structure under wind. Energy dissipation is applicable to a structure under both wind and earthquakes. The basic function of energy dissipation devices is that they can consume a portion of the input energy and thereby reduce the structural vibration when they are incorporated into a structure [2]. They include a wide range of damping devices and the most common ones are metallic dampers, viscoelastic dampers and viscous fluid dampers (VFDs), etc. The metallic dampers consume energy based on plastic yielding of metal materials so that they are more applicable to strong external excitations such as earthquakes and typhoons, which inevitably make the metal yield. Viscoelastic dampers consume energy based on the shear deformation of viscoelastic solids; they provide both additional damping and additional stiffness to the structure and thereby change the structural stiffness. It indicates that they are more applicable to structures requiring additional stiffness to resist lateral deformation. Compared with the two above-mentioned energy dissipation devices, VFDs have the advantage of being applicable to both strong external excitations such as earthquakes/typhoons and weak ones such as moderate wind. Moreover, the use of VFDs does not provide additional stiffness to the structure, thereby avoiding the unexpected change of the structural stiffness and natural vibration frequency, which is important in structural designs. The most two common types of vibration absorbers are the tuned mass damper (TMD) and the tuned liquid damper (TLD). The former absorbs energy based on the inertial force of mass and the latter absorbs energy based on the dynamic pressure of liquid. Comparatively speaking, TMDs are much more widely used in engineering structures than TLDs, since the former is a well-developed technique that is easier to design and construct. From the above descriptions, the use of VFDs as typical energy dissipation devices and TMDs as typical vibration absorbers to mitigate fatigue damage of welded beam-to-column connections is discussed in this paper.

There are two main fatigue analysis methods from the perspective of analysis procedures, which are the frequency domain analysis and the time domain analysis. The frequency domain analysis based on mode superposition considers the random nature of external loading and proves to be a reliable option with low computational expense and a simple computing model. For example, Janbazi and Tabeshpour [3] discussed the application of several configurations of viscous dampers on jackets and its effect on damage and fatigue lifetime by introducing a spectral method for assessment and rehabilitation of the jacket platform structure; Allen et al. [4] presented a computationally efficient frequency domain model for of a floating wind turbine with multiple hull-based TMDs; Repetto and Solari [5] analyzed the fatigue collapse of two slender structures due to wind-induced vibrations using frequency domain analysis. However, two distinguished shortcomings must be pointed out for this method. The first one is that the frequency domain analysis based on mode superposition does not suit nonlinear analysis. It is revealed in Section 2 that the damping force output by a VFD is nonlinearly related to the speed of the piston movement and, moreover, plastic strain is found near the welding location in the case of low-cycle fatigue damage, which means nonlinear analysis is indispensable. The second shortcoming is that the frequency domain analysis is not as applicable as the time domain analysis to the description of the local stress near the welding location, due to the complex geometry properties and the resulting serious stress concentration and nonlinear stress gradient. Based on the above two shortcomings, frequency domain analysis is obviously not the optimum option. On the contrary, the time domain analysis has the advantages of being suitable to nonlinear cases and being capable of describing the local stress near the welding location more precisely, while it has the disadvantages of high computational expense and a complex computing model, since the tedious time-history analysis and complex finite element models are almost inevitable. Therefore, it is thought that frequency domain analysis provides elegant solutions but is difficult to use in engineering applications, while time domain approaches allow classical fatigue analyses but require considerable computational

or experimental efforts [6]. From the above discussion, the time domain analysis proves to be a better option for the fatigue assessment of welded beam-to-column connections.

Based on the review of the related literature, some new real-time output-based solutions such as the real-time eigen perturbation strategies in structural health monitoring must be mentioned. These solutions can illustrate damage detection in an online mode with considerably less computational expense [7,8]. However, according to the latest literature, these solutions are mainly limited to damage detection including crack detection when dealing with fatigue damage problems [9] and have never been applied to the fatigue life assessment of engineering structures. Although they may have a promising future, the usability and availability of them in fatigue life assessment is still unclear and they are obviously not the main topic of this paper. Thus, the real-time output-based solutions are not discussed in the following paragraphs.

Vibration control is traditionally used in vibration response mitigation such as displacement and acceleration of buildings under wind and earthquakes. However, researchers have started to realize that passive vibration control can also be used in fatigue damage mitigation within the last two decades. Palmeri and Ricciardelli [10] estimated the fatigue life of structural components of high-rise buildings provided with viscoelastic dampers and found that viscoelastic dampers are effective in mitigating both the buffeting response and fatigue damage in medium-rise and high-rise buildings. Golafshani and Gholizad [11] evaluated the efficiency of an optimally designed tuned mass damper for fatigue damage mitigation in real steel jacket platforms and found that such dampers showed a great performance in this application. Ambrosio et al. [12] proposed an active control design to minimize fatigue damage on the structure from a theoretical, numerical and experimental point of view, which showed a significant improvement. Ripamonti et al. [13] proposed an adaptive vibration controller to increase the fatigue life of a smart structure made of composite material and actuated with piezoelectric patches. Andersson et al. [14] studied the use of passive and adaptive damping systems to mitigate vibrations in a railway bridge during resonance and to increase its fatigue service life.

However, there are still limitations in the abovementioned literature. Firstly, the above literature discussed the fatigue damage mitigation from a more global view of the whole structures, ranging from high-rise buildings and jacket platforms to railway bridges, but none of them discussed the fatigue damage mitigation of the more complex welded connections in structures, which are completely different from common components and whole structures. The welding part of a beam-to-column connection consists of three welded joints (the fillet welded joint connecting the beam web and the column flange, the butt welded joint connecting the top beam flange and the column flange and the butt welded joint connecting the bottom beam flange and the column flange) and two welding holes between them, as shown in Figure 1. The complex geometry properties lead to a serious stress concentration effect and nonlinear stress gradient near the local welding location. Consequently, a time domain fatigue analysis based on the computation of the local stress using a refined computational model is indispensable for a beam-to-column connection. On the contrary, the fatigue analysis of a common structure does not need to consider such local stress effects and the frequency domain fatigue analysis is more commonly used instead. Secondly, each of the above literature only focused on a single kind of vibration control system and lacks systematical comparison between common kinds of vibration control systems and, moreover, detailed discussions of the effect of technical parameters on the mitigation effect are still limited. Finally, when the external cyclic loading is large enough to result in plastic strain and low-cycle fatigue damage near the welding location, the elastoplastic analysis is required. However, the fatigue analysis of a global structure barely considers the effect of plastic strain, since in most cases, plastic strain is only found near the welding location and does not affect the behavior of the global structure. Therefore, the above literature mainly involves the use of vibration control in high-cycle fatigue damage mitigation, while low-cycle fatigue damage mitigation is barely discussed.

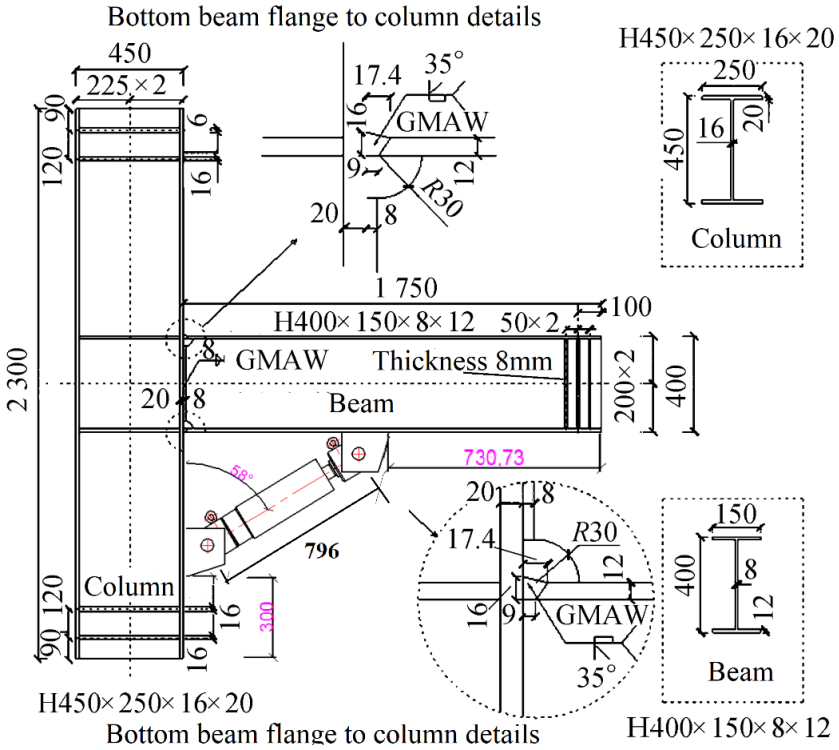

Figure 1. Welded beam-to-column connection.

The novelty of this research is to solve the above three current limitations. The fatigue damage mitigation of the welded beam-to-column connections in steel high-rise buildings is discussed and systematical comparisons of the two mitigation systems, including VFDs and TMDs, are made, with the effect of technical parameters on the mitigation effect being elaborated. Some original and unreported mitigation phenomena of the two vibration control systems are revealed and the use of them in low-cycle fatigue damage is also discussed for the first time. To the authors' knowledge, it is the first original research to discuss fatigue damage mitigation in welded beam-to-column connections.

In this paper, numerical study is conducted to research the use of two passive vibration control systems, VFDs and TMDs, in fatigue damage mitigation for welded beam-to-column connections in steel high-rise buildings. The fatigue damage mitigation is studied based on finite element analysis for the case of a single connection under constant amplitude cyclic loading in Section 2, which consists of three parts: the use of VFDs (Section 2.1), the use of TMDs (Section 2.2) and the condition of low-cycle fatigue damage (Section 2.3). In addition to the above fatigue assessment and the comparison of mitigation effects, a parametric study is also conducted to study the technical parameters of the two damping systems on the mitigation effect within Sections 2.1 and 2.2. The fatigue damage mitigation using the two damping systems for multi-connections in a steel high-rise building under the stochastic wind is introduced in Section 3, including the fatigue assessment, the comparison of mitigation effects and technical parametric study. In Section 4, discussion of important and unaddressed issues, including the optimization of damper positions and the negative mitigation effect, is made before the conclusions in Section 5 are drawn.

2. Fatigue Damage Mitigation for a Single Connection

2.1. Mitigation Using the VFD System

A VFD is a passive velocity-dependent damping device which works based on the damping force given by the interaction of the viscous medium (silicone oil) and the damper components. It is considered to only provide additional damping to the structure without

changing its rigidity or natural vibration period dramatically. Generally speaking, the damping force output by a VFD is described in Equation (1):

$$F_D = CV^{\alpha} \quad (1)$$

where F_D is the damping force; C is the damping coefficient; α is the damping exponent; V is the speed of the piston movement.

2.1.1. Formulation of the Model

A welded beam-to-column connection made of high-strength low-alloy structural steel GB Q345B, which is approximate to S355 in BS code, is discussed. The material properties of the steel are that the elastic modulus is 206 GPa, the Poisson's ratio is 0.3, the density is 7850 kg/m^3, the yield strength is 345 MPa and the tensile strength is 620 MPa. The detailed dimensions of the connection and weld details are all shown in Figure 1. The welding is conducted by the gas metal arc welding (GMAW) process in the form of the full penetration groove weld. Meanwhile, the VFD is connected to the connection as shown in Figure 1.

The three-dimensional finite element model of the connection without the VFD is established using an eight-node 3D solid structural element SOLID185 in the commercial software ANSYS, as shown in Figure 2a. The mesh is more refined near the weld detail with a mesh size of about 5 mm, while it becomes more sparse at locations far away from the weld detail at a mesh size of 13 mm, as shown in Figure 2b. Meanwhile, a model of the connection with a VFD is also established, as shown in Figure 2c. The VFD is modeled by COMBIN37, a kind of unidirectional spring damper element, and it connects the bottom of the beam flange with the lateral surface of the column web. The damping coefficient is C = 750 kN·s/m and the damping index is α = 0.25. To consider the role of the potential gusset plate and to avoid the extreme local stress concentration brought by the two ends of the VFD, a rigid region is generated by degree-of-freedom constraint equations between relate nodes at the two locations that the VFD connects. The degree of freedom of nodes at the top and the bottom of the column are all constrained. The constant amplitude cyclic loading as a sinusoidal wave with a force amplitude of ΔF = 60 kN, a stress ratio of $R = -1$ and a period of T = 24 s is exerted on the far end of the beam, as shown in Figure 2a. The bilinear kinematic hardening rule using von Mises plasticity (BKIN) is assumed for the steel.

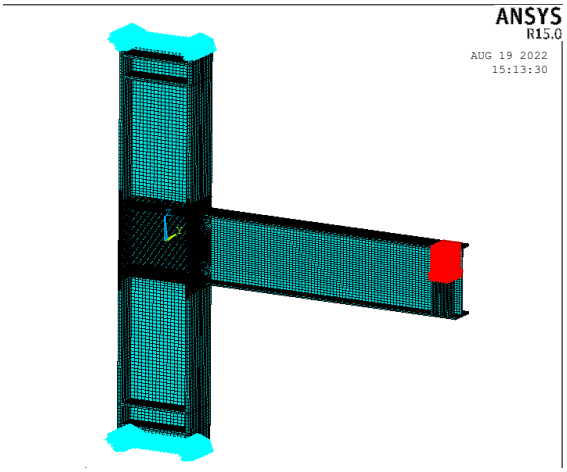

(**a**)

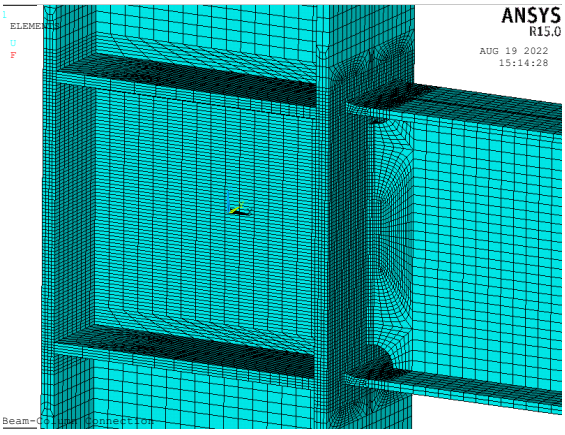

(**b**)

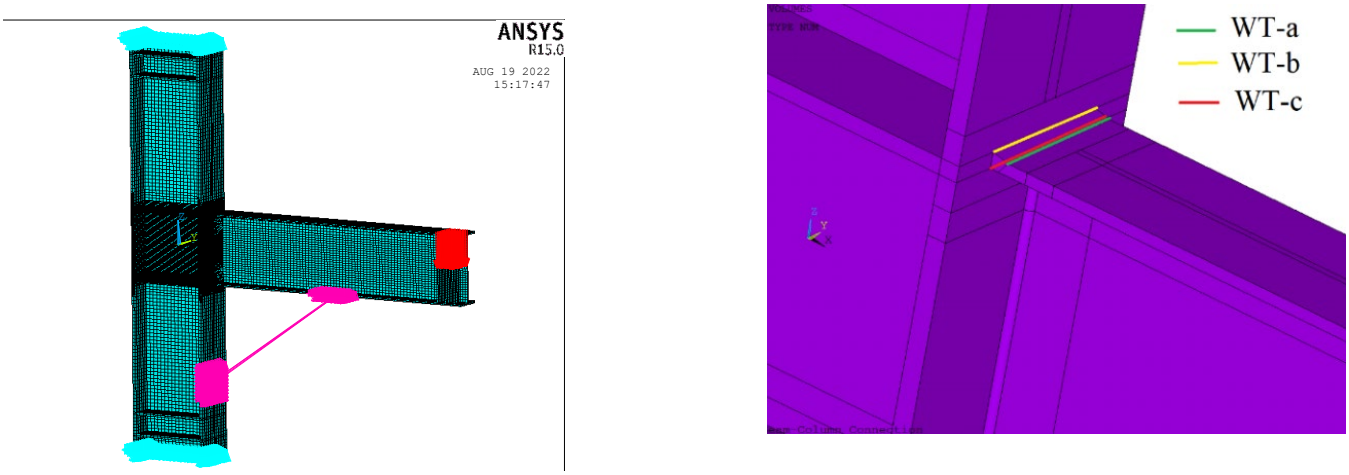

(**c**) (**d**)

Figure 2. Finite element model of the connection. (**a**) Connection without the VFD. (**b**) Local view of the weld detail. (**c**) Connection with the VFD. (**d**) Definition of weld toe lines.

2.1.2. Results and Analysis

The fatigue performance of this connection is strongly related to the stress amplitude at the weld detail. Thus, three weld toe lines of the weld seam connecting the top beam flange and the column are defined as shown in Figure 2d, where WT-a is the weld toe on the top beam flange, WT-b is the top weld toe on the column web and WT-c is the bottom weld toe on the column web. The maximum local principal stress $\sigma_{\text{L-max}}$ along the three weld toe lines in the connection with and without the VFD during the loading is, respectively, illustrated in Figure 3a,b. From the figures, it is found that the three weld toe lines show different stress distribution characteristics. The stress approximately presents an inverted V-shaped distribution along WT-a and the stress concentration is more serious at the center of the line, while it presents a W-shaped distribution along WT-b and WT-c, and the stress concentration is more serious at both the two sides and the center of the line. Moreover, it is found from the comparison of the figures that the maximum local principal stress along the weld toe decreases dramatically with the installation of the VFD for all the three weld toe lines, at a percentage of about 70%. It indicates that the VFD plays a great role in the mitigation of local stress near the weld detail.

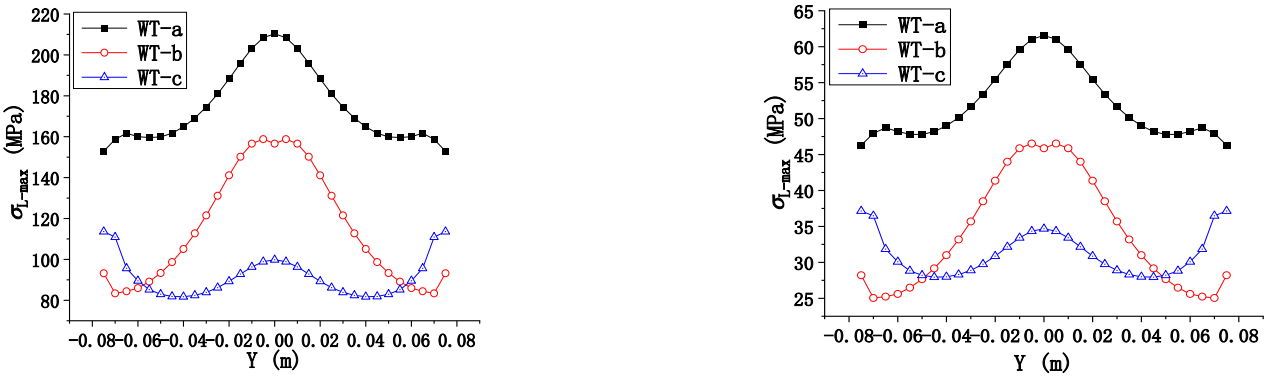

(**a**) (**b**)

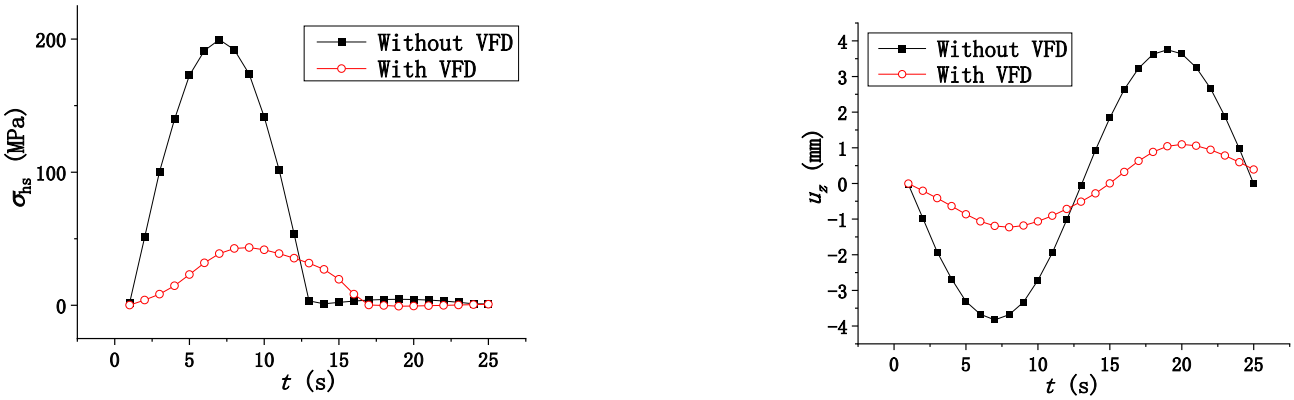

Figure 3. Stress and displacement of the connection with or without VFD. (**a**) Maximum local principal stress along the weld toe in the connection without the VFD. (**b**) Maximum local principal stress along the weld toe in the connection with the VFD. (**c**) Hotspot stress comparison. (**d**) Vertical displacement comparison.

The fatigue life of a component consists of fatigue crack initiation life and fatigue crack growth life. The fatigue crack initiation life is the life from the start of the cyclic loading to the appearance of visible cracks with a length of 1 mm [15], while the fatigue crack growth life starts from the appearance of these visible cracks to final ruptures of the component. Since the fatigue crack growth life is relatively short and it tends to be dangerous if final rupture is regarded as the failure criterion; the fatigue life discussed in this paper is the fatigue crack initiation life according to the suggestion made by the IIW recommendation (IIW2259-15) [16]. It is worth noting that instances of a sudden damage in a connection or a structure can lead to an abrupt change in the mass or stiffness. However, as soon as small visible cracks are found in welded beam-to-column connections, the fatigue analysis stops and there is no need to discuss the following events such as the abrupt change in the mass or stiffness, since visible cracks with a length of 1 mm in beam-to-column connections lead to little change in the structural mass or stiffness.

So far, the authors have conducted a series of research in fatigue assessment of welded beam-to-column connections using different fatigue assessment approaches, including the nominal stress approach, the hotspot stress approach, the equivalent structural stress approach, the notch stress approach and the theory of critical distances, etc. [17,18]. The detailed information and advantages/disadvantages of all these approaches can be found in the authors' previous publication [19]. Thus, it is necessary to decide proper fatigue assessment approaches for the connections in this paper. The finite element model of the single connection in this section is mainly established using SOLID elements and thus the nominal stress is not a good option, since the abstraction of the nominal stress from the analysis results is not as easy as that in a model established using BEAM elements. The notch stress approach and the theory of critical distances are two approaches based on local stress, so that they both require very refined mesh sizes in the finite element model and thus take a tedious amount of computing time and expends tremendous computing resources. Since there are numerous computing conditions involved and the computation of models with VFDs even requires time-consuming nonlinear analysis, these two approaches are also not the best options. The two approaches left are the equivalent structural stress approach and the hotspot stress approach. Although the former has the advantage of being insensitive to mesh size and requires only one S-N curve, it is more effective in finite element models using SHELL elements and the abstraction of the membrane stress and the bending stress require an integral calculation in models using SOLID elements, while the calculation using the latter model is more efficient, especially in the computation of numerous computing conditions. Thus, the hotspot stress approach is selected as the proper

approach for the single connection in this section. On the contrary, all the approaches except the nominal stress approach are not very applicable to the multi-connections of a structure in Section 3, since these approaches all require models using SOLID or SHELL elements. It is true that the use of a multi-scale finite element model may be the solution to this problem. However, fatigue analysis needs to be conducted within numerous connections in Section 3 and it is nearly impossible to establish a multi-scale finite element model for so many connections. Therefore, the fatigue assessment for the multi-connections in a high-rise building is conducted using the nominal stress approach. It is worth noting that the above discussion is mainly for the connections under high-cycle fatigue damage. Plastic strain is found near the welding location under low-cycle fatigue damage; therefore, the local stress–strain approach is the best option.

The hotspot stress represents the structural stress at the hotspot location, i.e., the weld toe location, which includes all stress-raising effects of a structural detail. It is determined on the surface at the hotspot (weld toe) of the component to be assessed using two reference points, the location $0.4t$ and $1.0t$ away from the weld toe, to extrapolation to the weld toe location [16]. The hotspot stress σ_{hs} is calculated as Equation (2):

$$\sigma_{\mathrm{hs}} = 1.67\sigma_{0.4t} - 0.67\sigma_{1.0t} \tag{2}$$

where $\sigma_{0.4t}$ and $\sigma_{1.0t}$ are the stresses of the location $0.4t$ and $1.0t$ away from the weld toe and t is the plate thickness. The stress results in these two locations can be easily abstracted from the finite element analysis results. After the hotspot stress range $\Delta\sigma_{\mathrm{hs}}$ under the cyclic loading is obtained, the fatigue life is calculated using the S-N curve, as shown in Equation (3):

$$(\Delta\sigma_{\mathrm{hs}})^{m_0} N = C_0 \tag{3}$$

where m_0 and C_0 are parameters of the S-N curve, dependent on the type of the welded connection. According to IIW recommendations (IIW2259-15) [16], FAT90 is the most suitable S-N curve for this connection, where $C_0 = 4.046 \times 10^{15}$ and $m_0 = 5$ when $\Delta\sigma_{\mathrm{hs}} \leq 52.7$ MPa (knee point of the S-N curve), while $C_0 = 1.458 \times 10^{12}$ and $m_0 = 3$ when $\Delta\sigma_{\mathrm{hs}} > 52.7$ MPa. From the brief introduction above to the hotspot stress approach, it is clear that this approach uses the stress obtained by extrapolation from the two reference points to the weld toe as the key stress index (hotspot stress) and thus the fatigue life is calculated from this key stress index based on an S-N curve specified by IIW recommendations.

The hotspot stress σ_{hs} near WT-a, with more serious stress concentration than the other two weld toe lines, within one cycle of loading is shown in Figure 3c. Meanwhile, the far-end vertical displacement of the beam u_z is illustrated in Figure 3d. It is found from the figures that the hotspot stress and the vertical displacement are both considerably decreased by about 70% during the cycle of loading and the two indexes show similar and synchronous mitigation trends that show a better vertical displacement mitigation effect along with a better stress mitigation effect. Moreover, it is found that the two indexes decrease dramatically from the beginning of the cyclic loading, which means that the VFD takes effect instantly with the external loading. Meanwhile, it is worth noting that the hotspot stress and the vertical displacement results of the connection with the VFD show a phase difference of about $\pi/12$ lagging behind those of the connection without the VFD. It indicates that the use of the VFD changes the phase property of the structural responses (output sinusoidal wave).

The fatigue life is then calculated based on the hotspot stress range by Equation (3) and a fatigue life ratio k is defined as shown in Equation (4):

$$k = N_e / N_0 = T_e / T_0 \tag{4}$$

where N_0 and N_e are the fatigue life of the connection without and with the passive control system, and T_0 and T_e are their counterparts expressed in the unit of a year, which is used in Section 3. It is obvious that a larger k value indicates a better fatigue damage mitigation

effect and fatigue life prolonged effect. The result is listed in the first row of Table 1. It is found that a k value of 15 is obtained so that the fatigue life is prolonged considerably with the installation of the VFD.

2.1.3. Parametric Study

To better understand the effect of the two technical parameters, the damping coefficient C and the damping exponent α on the mitigation effect of both the hotspot stress and vertical displacement, simultaneously, the double Y-axis plot is established as shown in Figure 4a,b. The Y-axis on the left side indicates the hotspot stress range $\Delta\sigma_{hs}$ and that on the right side shows the absolute value of the far-end vertical displacement of the beam, $|u_z|$. The variation trend of both the two indexes with the damping coefficient and the damping exponent is plotted. It is found from Figure 4a,b that both the hotspot stress range and the far-end displacement decrease with the increase in the damping coefficient and they increase with the increase in the damping exponent. The two indexes show similar and synchronous mitigation trends for all the parameter conditions, which coincides with the phenomenon found in Figure 3c,d. It indicates that the two optimal technical parameters which contribute to the maximum structural vibration response mitigation effect also lead to the maximum fatigue damage mitigation effect. This conclusion is rather constructive to the design of passive control systems in high-rise buildings, since the optimal technical parameters for the damping systems simultaneously lead to the most effective mitigation of both the stress (fatigue damage) and the vibration responses (displacement) in a structure.

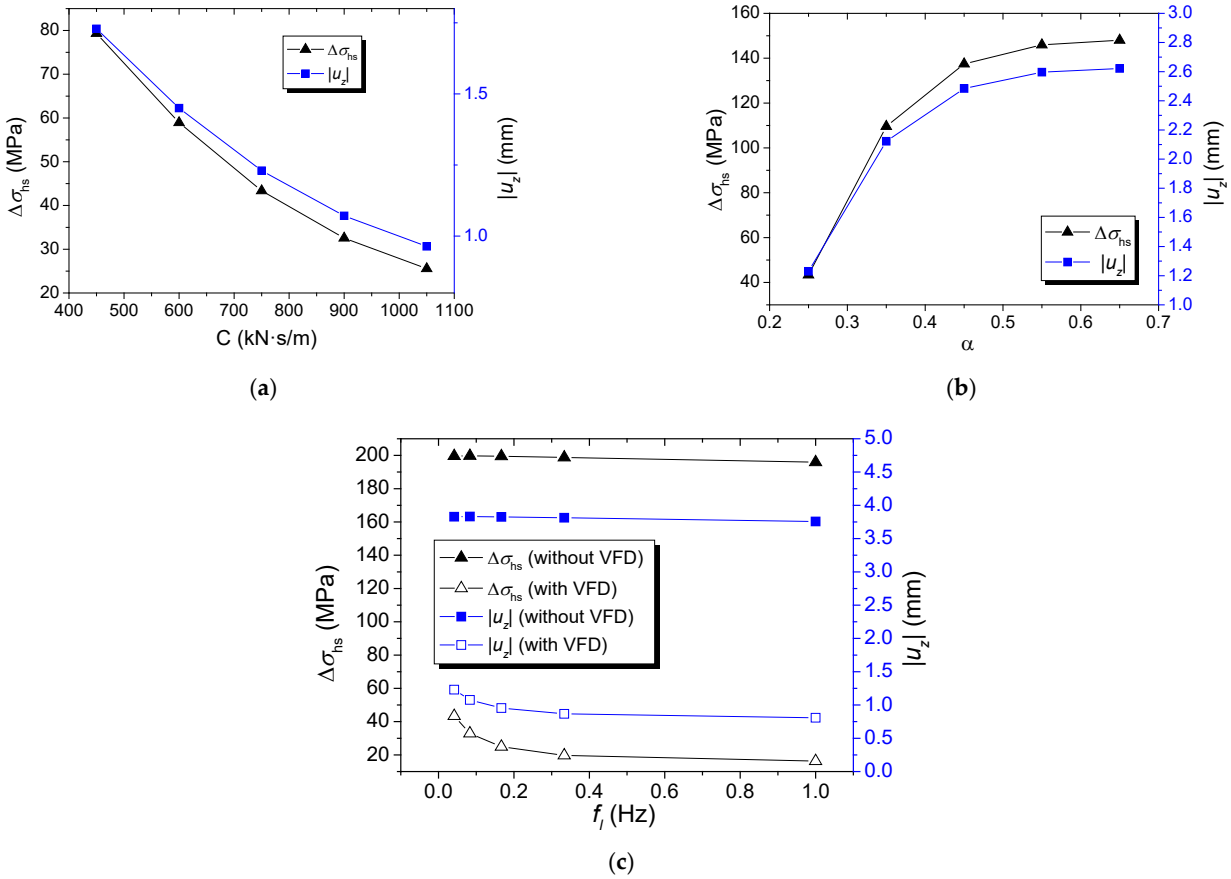

Figure 4. Effect of parameters on hotspot stress range results of the connection with and without the VFD. (**a**) The effect of the damping coefficient. (**b**) The effect of the damping exponent. (**c**) The effect of the loading frequency.

Table 1. Results of the connection with and without the VFD.

Condition No.	Parameters				Without the VFD			With the VFD			
	T (s)	f_l (Hz)	α	C (kN·s/m)	$\Delta\sigma_{hs}$ (MPa)	$\lvert u_z \rvert$ (mm)	N_0	$\Delta\sigma_{hs}$ (MPa)	$\lvert u_z \rvert$ (mm)	N_e	k
1	24	0.042	0.25	450	196.86	3.83	1.911×10^5	79.34	1.73	2.920×10^6	15
2	24	0.042	0.25	600				58.94	1.45	7.122×10^6	37
3	24	0.042	0.25	750				43.37	1.23	2.638×10^7	138
4	24	0.042	0.25	900				32.55	1.07	1.108×10^8	580
5	24	0.042	0.25	1050				25.56	0.96	3.705×10^8	1939
6	24	0.042	0.35	750				109.58	2.12	1.108×10^6	6
7	24	0.042	0.45	750				137.46	2.48	5.613×10^5	3
8	24	0.042	0.55	750				145.96	2.60	4.689×10^5	2
9	24	0.042	0.65	750				148.03	2.62	4.495×10^5	2
10	12	0.083	0.25	750	199.59	−3.828	1.834×10^5	43.37	1.230	2.638×10^7	144
11	6	0.167	0.25	750	199.72	−3.831	1.830×10^5	32.91	1.075	1.047×10^8	572
12	3	0.333	0.25	750	199.48	−3.826	1.837×10^5	24.94	0.953	4.193×10^8	2283
13	1	1.000	0.25	750	198.80	−3.813	1.856×10^5	19.73	0.868	1.352×10^9	7286

It is well-known to all that the effect of a VFD is strongly related to the relative moving velocity between its two ends and thus the mitigation effect with the loading frequency f_l is also discussed. The similar double *Y*-axis plot is illustrated in Figure 4c. It is found that the hotspot stress range and the far-end displacement of the connection without the VFD is not obviously affected by the loading frequency, while those of the connection with the VFD both decrease with the increase in the loading frequency nonlinearly. It can be explained by the fact that a larger loading frequency leads to larger relative velocity between the two ends of the VFD and finally gives rise to a better mitigation effect due to its velocity dependence.

The fatigue life and its prolonged effect for all the parameter conditions are listed in Table 1, where Conditions No. 1–5 show the effect of the damping coefficient, Conditions No. 6–9 give the effect of the damping exponent and Conditions No. 10–13 indicate the effect of the loading frequency. It is found that the *k* value varies dramatically in different conditions, which can even reach hundreds or thousands. It reveals that the use of a VFD is extremely effective in fatigue damage mitigation and it is more effective in the connection with a large damping coefficient and a small damping exponent under cyclic loading with a high frequency.

2.2. Mitigation Using the TMD System

The TMD system consists of a main structure and a substructure attached to it. The substructure contains masses, springs and dampers, so that it has the properties of mass, stiffness and damping. A typical SODF (Single Degree of Freedom) structure with a TMD is shown in Figure 5a. The natural frequency of the substructure is adjusted to be close to that of the main structure by changing its mass and stiffness. When the main structure vibrates under the external load, the substructure outputs an inertial force opposite to the vibration direction of the main structure and thus the kinetic energy of the main structure is dissipated through the damping of the substructure to obtain a mitigation effect.

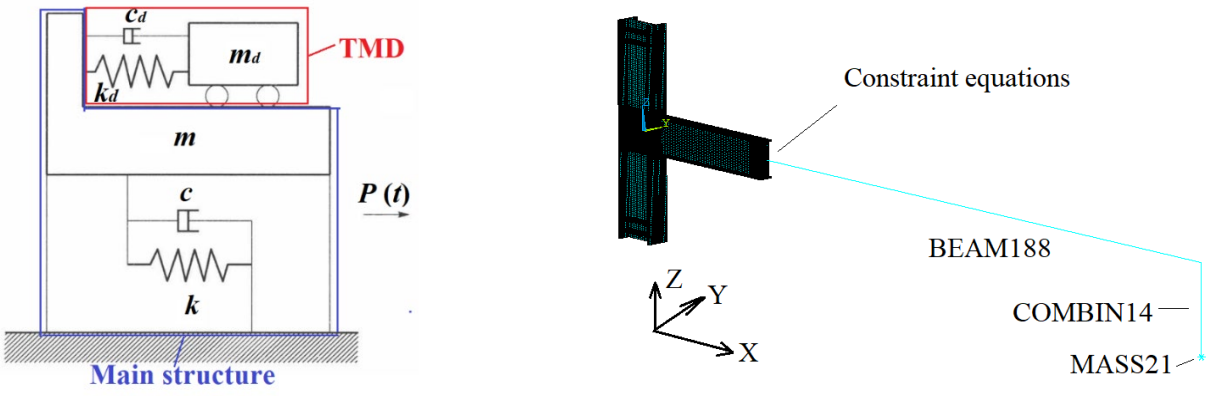

(**a**) (**b**)

Figure 5. Mechanical model and finite element model of the structure or connection with a TMD. (**a**) Mechanical model of a SODF structure with a TMD. (**b**) Finite element model of the connection with a TMD.

2.2.1. Formulation of the Model

The finite element model of the connection without the TMD is defined as Model A and it keeps the same as that without the VFD in Section 2.1. A model analysis is conducted first to show the vibration modes of the connection and the results of the first three primary vibration modes are given in Table 2. It is found from Table 2 that the frequency of the third vibration mode is 104.79 Hz and this mode, as the first order of translation in the *Z*-axis, is the same vibration pattern as that under the cyclic loading. It is obvious that this vibration mode is too rigid for mitigation using the TMD, since it has been pointed out that a TMD works with better effect in flexible structures than in rigid structures [2,20].

Thus, the frequency of this connection is adjusted to make it more flexible by increasing the beam length by a factor of four so that the beam length is 1.65 × 4 = 6.6 m, while other dimensions and boundary conditions remain unchanged. Due to limited computing resources, a multi-scale finite element model defined as Model B is established as shown in Figure 5b. The lengthened part of the beam is simulated by BEAM188, a kind of 3D two-node beam element, and it is connected to the original beam using degree-of-freedom constraint equations. The mass part of the TMD simulated using MASS21, a kind of structural mass element with six degrees of freedom, is connected through COMBIN14, a kind of spring damper element, to the bottom of the beam far-end location where the largest vertical displacement of the third vibration mode is reached. The first three vibration modes are calculated and listed in Table 2, which are the first order of translation in the *Y*-axis, the first order of rotation around the *X*-axis and the first order of translation in the *Z*-axis. Thus, the cyclic loading is a sinusoidal wave with a force amplitude of ΔF = 6 kN, a stress ratio of $R = -1$ and a frequency of 6.31 Hz exerted on the far end of the beam in Model B, while the similar cyclic loading with a force amplitude of ΔF = 60 kN, a stress ratio of $R = -1$ and a frequency of 104.79 Hz is exerted on Model A, so that the frequency of the cyclic loading keeps almost equal to that of the third vibration mode of both Model A and Model B to make the TMD work with great efficiency.

Table 2. Frequency of models and parameters of the TMD.

Model	Modal Frequency (Hz)			Parameters of the TMD							
	1	**2**	**3**	m_d **(kg)**	m **(kg)**	μ	$r_{f\text{opt}}$	ξ_{opt}	f_d **(Hz)**	C_{opt} **(N·s/m)**	k_{opt} **(N/m)**
A	22.13	41.39	104.79	9.34	467.06	0.02	0.98	0.086	106.89	1075.87	4.21×10^6
B	1.30	4.67	6.31	15.99	799.47	0.02	0.98	0.086	6.44	110.96	2.62×10^4
C	0.396	0.417	0.468	2.305×10^7	1.152×10^6	0.05	0.952	0.134	0.416	8.040×10^5	7.854×10^6
D	0.390	0.427	0.452	-	-	-	-	-	-	-	-

Den Hartog [21] suggested the optimal technical parameters of a TMD such as the optimal frequency ratio $r_{f\text{opt}}$, the optimal damping ratio ξ_{opt}, the optimal spring stiffness k_{opt} and optimal damping coefficient C_{dopt}. They are calculated using Equations (5)–(8) [20,22]:

$$r_{f\text{opt}} = 1/(1+\mu) \tag{5}$$

$$\xi_{\text{opt}} = \sqrt{\frac{3\mu}{8(1+\mu)}} \tag{6}$$

$$k_{\text{opt}} = r_{f\text{opt}}^2 \omega^2 m_d \tag{7}$$

$$C_{\text{dopt}} = 2\xi_{\text{opt}} r_{f\text{opt}} \omega m_d \tag{8}$$

where the frequency ratio r_f is the ratio of the frequency of the TMD f_d to that of the structure f, as $r_f = f_d/f$, the mass ratio μ is the ratio of the mass of the TMD m_d to that of the structure m, as $\mu = m_d/m$, the damping ratio of TMD ξ is expressed as $\xi = c_d/(2m_d\omega_d)$ and c_d is the damping coefficient of the TMD and ω_d is the circular frequency of the TMD. According to Equations (5)–(8), the optimal parameters for the TMD in both models are calculated and listed in Table 2.

The time-history analysis is conducted, respectively, for Model A and Model B, and the hotspot stress of WT-a and the vertical displacement at the far end of the beam are illustrated in Figure 6. It is found that the TMD designed with the optimal parameters suggested by Den Hartog has little effect on the hotspot stress and vertical displacement results in Model A, while it decreases both the hotspot stress and displacement results distinctly in Model B, at a percentage rate of 10–15%. This phenomenon proves that the TMD works with greater efficiency in flexible structures than in rigid structures and it is the reason why Model A needs to be adjusted to Model B. It is also found that the hotspot

stress and the far-end vertical displacement show similar and synchronous mitigation trends that show a better vertical displacement mitigation effect along with a better stress mitigation effect, which is the same as the phenomenon found in the connection with the VFD. Moreover, the equipment of the TMD causes little phase difference from the original phase in the two indexes, as shown in Figure 6c,d, and the TMD starts to take effect from the second cycle and reaches the greatest efficiency from the third cycle. This phenomenon is completely different from the equipment of the VFD, which causes phase difference from the original phase in the two indexes, and it starts to work instantly from the first cycle. It may stem from the fact that the mitigation of the TMD takes effect due to the inertial force generated by its vibration, and the vibration is relatively weak in the first cycle and becomes stronger and reaches a stable vibration stage at the second or third cycle when the TMD takes effect.

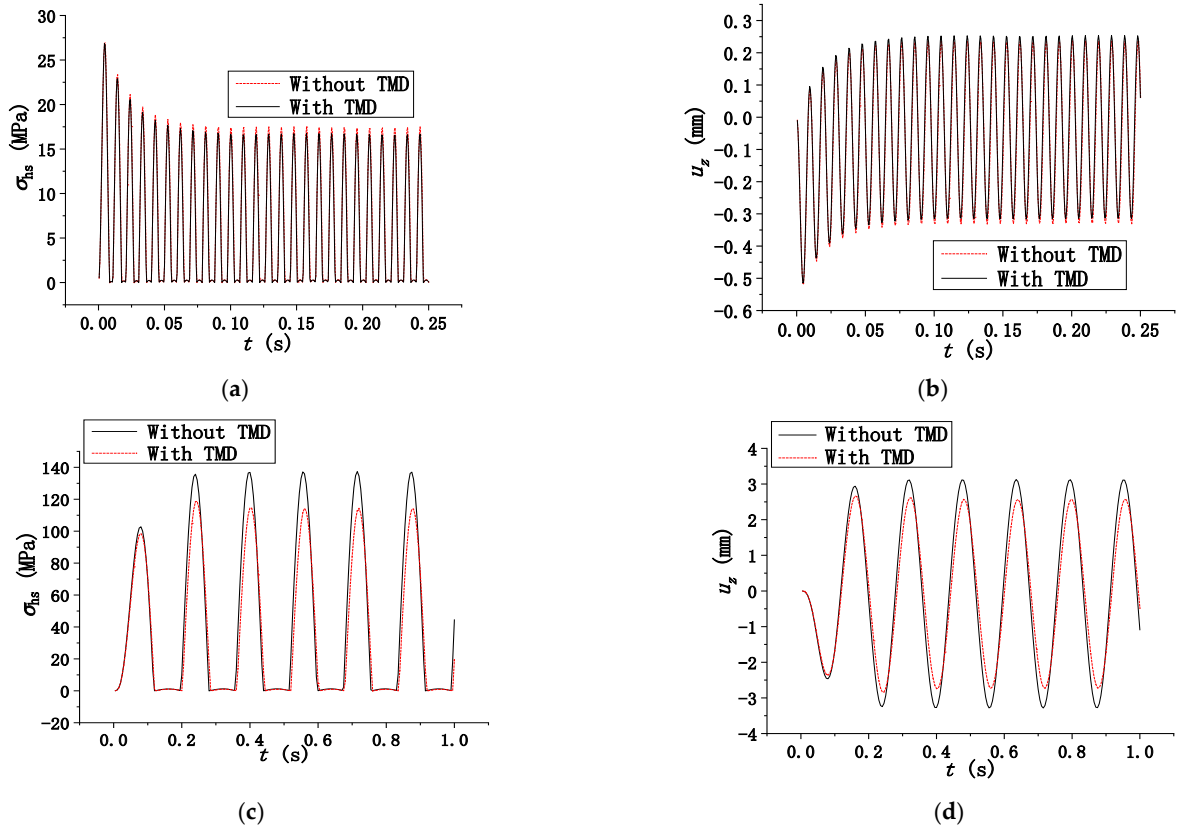

Figure 6. Time-history results of Model A and Model B. (**a**) Hotspot stress time-history of Model A. (**b**) Far-end vertical displacement of Model A. (**c**) Hotspot stress time-history of Model B. (**d**) Far-end vertical displacement of Model B.

2.2.2. Parametric Study

The effect of technical parameters such as the frequency ratio, the damping ratio and the mass ratio on the mitigation effect are all considered and the detailed results are illustrated in the double *Y*-axis plot in Figure 7 and listed in Table 3, where Conditions No. 1–7 show the effect of the frequency ratio, Conditions No. 8–12 indicate the effect of the damping ratio and Conditions No. 13–16 present the effect of the mass ratio.

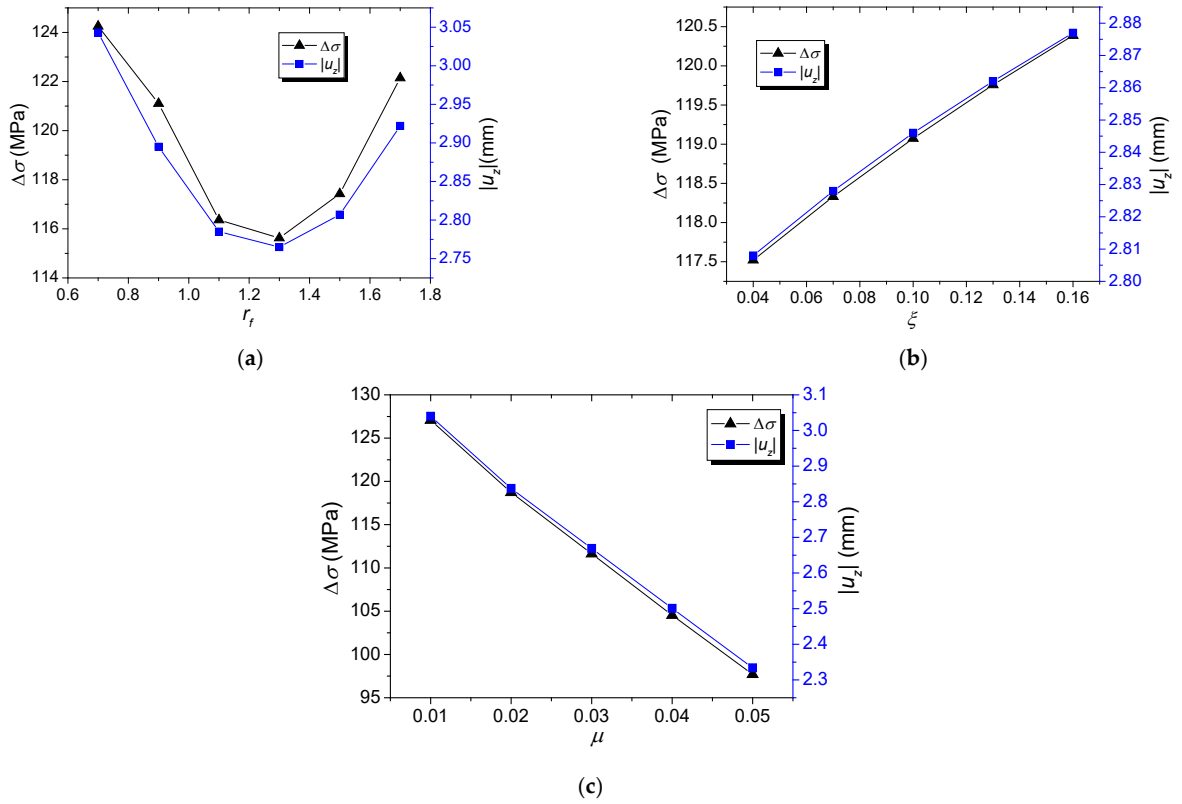

Figure 7. Effect of parameters on hotspot stress range results of the connection with and without the TMD. (**a**) Effect of the frequency ratio. (**b**) Effect of the damping ratio. (**c**) The effect of the mass ratio.

It is found that the mitigation effect decreases with the increase in frequency ratio until it reaches a minimum value; it starts to increase after that, when the damping ratio keeps constant at 0.086. It indicates that there is indeed an optimal frequency ratio for the TMD; therefore, the design of the TMD should be based on it. It is worth noting that the optimal frequency ratio for this TMD is about 1.3, which is only the optimal value for this specific loading frequency (6.31 Hz). It is completely different from the optimal frequency ratio of 0.98 proposed by Den Hartog, which is the optimal frequency ratio considering series of loading frequencies.

The hotspot stress increases almost linearly with the increases in the damping ratio when the frequency ratio keeps constant at 0.98, which indicates that the damping ratio leads to the decrease in the mitigation effect under such a frequency ratio. Meanwhile, the hotspot stress decreases almost linearly with the increase in the mass ratio when the damping ratio and the frequency ratio both keep constant, indicating that the increase in the TMD mass generally contributes to a better mitigation effect. However, it is impossible to increase it infinitely, since the overweight TMD increases the bending moment and shear force within the beam and causes potential failure danger. Thus, a mass ratio of 0.02–0.05 is often adopted by engineering designs.

Based on the hotspot stress results, the fatigue life and its ratio are calculated for all the parameter conditions of the TMD, as shown in Table 3. It is found that the fatigue life ratio generally ranges from 1 to 3. Although the connection with the TMD has a longer beam length and more flexible stiffness than that with the VFD and they are not the same connection; the fatigue life ratios of the connection with the VFD are still considerably larger than those with the TMD, based on the comparison of Tables 2 and 3. It indicates that the use of a VFD in a single welded beam-to-column connection generally has a better fatigue damage mitigation effect than the use of a TMD, and it has better usability and takes effect instantly, for the VFD is suitable for connections with any stiffness, while the TMD is suitable to more flexible connections with a relatively low natural frequency.

Table 3. Results of the connection with and without the TMD.

Condition No.	Parameters			Without the TMD			With the TMD			
	μ	r_f	ξ	$\Delta\sigma_{hs}$ (MPa)	$\lvert u_z \rvert$ (mm)	N_0	$\Delta\sigma_{hs}$ (MPa)	$\lvert u_z \rvert$ (mm)	N_e	k
1	0.02	0.98	0.086	137.326	3.28	5.630×10^5	118.729	2.837	8.711×10^5	1.5
2	0.02	0.70	0.086				124.254	3.040	7.600×10^5	1.3
3	0.02	0.90	0.086				121.105	2.900	8.209×10^5	1.5
4	0.02	1.10	0.086				116.362	2.790	9.254×10^5	1.6
5	0.02	1.30	0.086				115.626	2.770	9.432×10^5	1.7
6	0.02	1.50	0.086				117.425	2.810	9.005×10^5	1.6
7	0.02	1.70	0.086				122.144	2.920	8.001×10^5	1.4
8	0.02	0.98	0.040				117.521	2.808	8.983×10^5	1.6
9	0.02	0.98	0.070				118.331	2.828	8.800×10^5	1.6
10	0.02	0.98	0.100				119.074	2.846	8.636×10^5	1.5
11	0.02	0.98	0.130				119.757	2.862	8.489×10^5	1.5
12	0.02	0.98	0.160				120.387	2.877	8.356×10^5	1.5
13	0.01	0.98	0.086				127.076	3.040	7.105×10^5	1.3
14	0.03	0.98	0.086				111.636	2.669	1.048×10^6	1.9
15	0.04	0.98	0.086				104.534	2.501	1.276×10^6	2.3
16	0.05	0.98	0.086				97.699	2.334	1.563×10^6	2.8

2.3. Low-Cycle Fatigue

The above research mainly discusses the condition of high-cycle fatigue damage. However, welded beam-to-column connections may suffer damage under potential earthquakes, which can be classified as low-cycle fatigue damage. Since it was demonstrated that a VFD is more effective in fatigue damage mitigation than a TMD in the previous two sections, the use of the VFD is taken as an example to discuss its effectiveness in low-cycle fatigue damage mitigation.

The elastoplastic time-history analysis is conducted. Since the connection may suffer plastic deformation under low-cycle fatigue damage, the cyclic displacement loading with a displacement amplitude of Δd = 6 mm and a displacement ratio of $R = -1$ is exerted on the far end of the beam instead of the cyclic force loading, and the wave type and period remain the same. The local plastic strain near the weld detail of the connection with and without the VFD is shown as a contour map in Figure 8. It is found that the plastic strain near the weld detail decreases or even disappears with the equipment of the VFD.

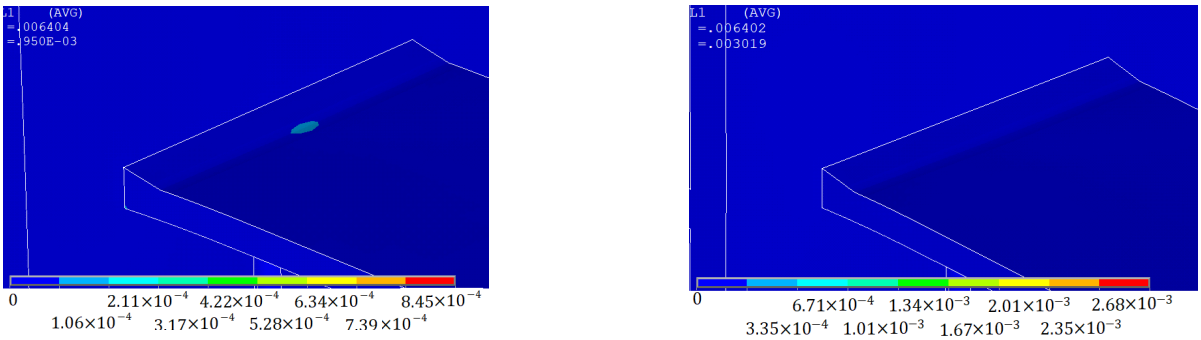

(**a**) (**b**)

Figure 8. Contour map of the local plastic strain. (**a**) Connection without the VFD. (**b**) Connection with the VFD.

The fatigue assessment of a welded connection under low-cycle fatigue needs to be conducted using the local stress–strain approach, instead of the hotspot stress approach, due to the existence of plastic strain. This approach is proposed by Socie [23], based on the assumption that the fatigue life of a welded specimen is the same as that of a smooth specimen if the stress–strain time history of the two specimens is the same. The fatigue life is calculated using the Coffin–Manson Equation, as shown in Equation (9):

$$2N = \left[\frac{\frac{\sigma'_f}{E}(2N)^{b-c} + \varepsilon'_f}{\frac{\Delta\varepsilon}{2}} \right]^{-\left(\frac{1}{c}\right)} \tag{9}$$

where σ'_f, ε'_f, b and c are four material-dependent parameters and they are 949 MPa, 0.159, −0.103 and −0.467 for the steel GB Q345B; $\Delta\varepsilon/2$ is the local strain amplitude. The results of the connections with and without the VFD using the damping coefficient C and the damping exponent α are listed in Table 4.

It is found from Table 4 that the fatigue damage mitigation of the connection with the VFD under the low-cycle fatigue condition is not as effective as that under the high-cycle fatigue condition, where the fatigue life ratio k is mainly about 2, while that in the high-cycle fatigue can reach even hundreds and thousands. The main reason may be that the increase in the stress slows down and reaches a stable stage in the stress–strain curve of the material due to the yield of the steel and the plastic strain, so that the local stress and strain in the connection with the VFD does not seem to vary a lot from that in the connection without the VFD. This may lead to the decreased fatigue life prolonging effect. Meanwhile, it is also found that the fatigue damage mitigation effect in the low-cycle fatigue is not greatly

affected by the damping coefficient or the damping exponent, indicating that it is not sensitive to the change of technical parameters. This phenomenon is completely different from that in the high-cycle fatigue condition.

Table 4. Results of the connection with and without the VFD under low-cycle fatigue.

Condition No.	Parameters		Without the VFD			With the VFD			
	α	C (kN·s/m)	$\Delta\varepsilon$ (1×10^{-3})	u_z (mm)	N_0	$\Delta\varepsilon$ (1×10^{-3})	u_z (mm)	N_e	k
1	0.25	450	2.034	−6.35	58,256	1.840	−6.32	92,129	1.6
2	0.25	600				1.833	−6.32	93,801	1.6
3	0.25	750				1.828	−6.32	95,020	1.6
4	0.25	900				1.824	−6.32	96,011	1.6
5	0.25	1050				1.819	−6.32	97,269	1.7
6	0.35	750				1.844	−6.32	91,192	1.6
7	0.45	750				1.852	−6.32	89,355	1.5
8	0.55	750				1.854	−6.32	88,904	1.5
9	0.65	750				1.855	−6.32	88,679	1.5

3. Fatigue Damage Mitigation for Multi Connections in the Structure

3.1. Finite Element Model

A high-rise building located in a coastal city susceptible to severe wind disasters in China is taken as an example of a steel braced-frame structure. The building has an ellipse plane shape with a long axis of 59.4 m and a short axis of 22.02 m, as shown in Figure 9a. It has 27 floors above ground, with a building height of 96 m. The hot-rolled H-sectional beams and box-sectional columns made of structural steel GB Q345B are connected by welded connections, where all the welding is conducted in the form of the full penetration groove weld. The sections of the columns on the first floor are Z1(600 × 600 × 45 × 45), Z2(600 × 850 × 50 × 50), Z3(600 × 700 × 40 × 40), Z4(600 × 600 × 50 × 50), Z6(600 × 600 × 53 × 53) and Z9(700 × 700 × 65 × 65), as shown in Figure 9a (Unit: mm). The beams on the first floor are mainly with a section of H500 × 200 × 10 × 16 and H588 × 300 × 12 × 20 (Unit: mm). The sectional areas of beams and columns gradually decrease on higher floors. The braces are mainly of a section of H428 × 407 × 17.5 × 35 (Unit: mm). The floor plate, with a thickness of 120 mm, is made of the constructional concrete GB C30 with an elastic modulus of 30 GPa and a Poisson's ratio of 0.2. The material property of GB Q345B is referred to in Section 2.1.1. The finite element model is established in the ANSYS software, as shown in Figure 9b. The beams, columns and braces are all simulated using BEAM188, a type of 3D two-node beam element and floors are simulated by SHELL63, a type of four-node shell element, at a mesh size of 2 m. To better validate this finite element model, the model of the same structure is established in another finite element analysis software, ETABS, as shown in Figure 9c. The natural vibration frequency results of the first three vibration modes are listed in Table 2 as those of Model D and they are compared with those of the model established in ANSYS as Model C in the same table. The discrepancy of the frequency results of the first three vibration modes between the two models is 1.15%, 2.39% and 3.34%, respectively, and they are all within a discrepancy limit of 5%. It demonstrates that the established finite element model in ANSYS is valid in the establishment of the model.

Stochastic fluctuating wind time series with a duration of 50 s and a time interval of 0.1 s to calculate wind-induced fatigue are generated based on the Davenport power spectrum using the harmonic superposition method [24], as shown in Equations (10) and (11):

$$\frac{nS_v(n)}{\overline{v}_{10}^2} = \frac{4k_r x^2}{n(1+x^2)^{3/4}} \tag{10}$$

$$x = 1200\frac{n}{\overline{v}_{10}} \tag{11}$$

where $\overline{v}_{10}$ is the reference wind speed taken as 21.43 m/s, calculated from the reference wind pressure in this area suggested by Chinese code for structural design (GB50009-2019), with a reference height of 10 m, a time interval of 10 min and a return period of 50 years; n is the frequency of the fluctuating wind; k_r is the terrain roughness factor of this area, which is 0.22; $S_v(n)$ is the power spectrum of velocity fluctuation. The simulated wind speed time series are converted into the frequency domain and they are compared with the Davenport spectrum. The typical fluctuating wind speed time series at the height of the first floor is shown in Figure 9d and it was found that the spectrum of the simulated wind time series agrees with the Davenport spectrum well in most frequency bands, as illustrated in Figure 9e.

Wind loads are only applied in the Y-axis direction of the structure. The total wind speed time series at the location of the j-th connection on the i-th floor, as $V_{ji}(z,t)$, which consist of the mean wind speed $\overline{v}_{ji}(z)$ and fluctuating wind speed $v_{ji}(z,t)$, are converted into the wind pressure time series $W_{ji}(z,t)$ according to Bernoulli's theorem, where z is the height of the i-th floor and t is the time. Subsequently, the wind pressure time series are converted into the concentrated wind force time series $P_{ji}(t)$ by multiplying the loading area A_{ji} of each beam-to-column connection on the windward surface of the building. The definition of the loading area can be found in an earlier publication by the authors [17]. The above conversion of the wind speed time series to the concentrated wind force time series is summarized as Equation (12):

$$\begin{aligned} P_{ji}(t) = A_{ji}\mu_s W_{ji}(z,t) = \tfrac{1}{2}A_{ji}\mu_s\rho {V_{ji}}^2(z,t) = \tfrac{1}{2}A_{ji}\mu_s\rho\left[\overline{v}_{ji}(z) + v_{ji}(z,t)\right]^2 \\ \approx \tfrac{1}{2}A_{ji}\mu_s\rho{\overline{v}_{ji}}^2(z) + A_{ji}\mu_s\rho\overline{v}_{ji}(z)v_{ji}(z,t) \end{aligned} \tag{12}$$

where ρ is the air density; μ_s is the shape coefficient of the structure, suggested by Chinese code (GB50009-2019) as 1.1. Only the buffeting response is considered, since this building does not have a very slender structure.

3.2. Fatigue Analysis

The time-history analysis is conducted and the beam-to-column connections on the 11th floor with the maximum interlayer displacement ratio are the connections for the fatigue analysis. The calculation process and results of the interlayer displacement ratio of each floor are not detailed due to limited pages. Since the columns and beams are all simulated using the beam element, the fatigue assessment is conducted using the nominal stress approach. Nominal stress σ_{nom} is the sectional stress calculated based on the internal forces on the component section away from the welded joint, where the local stress-raising effects do not exist, as shown in Equation (13):

$$\sigma_{\text{nom}} = \frac{N_{\text{c}}}{A} + \frac{M_X}{W_X} + \frac{M_Z}{W_Z} \tag{13}$$

where N_{c} is the axial force, A is the sectional area of the beam in the Y-axis direction, M_X and M_Z are the moment around X-axis and Z-axis, and W_X and W_Z are the section modulus around X-axis and-Z axis. The directions of the axes are shown in Figure 9a.

The nominal stress spectrums (cumulative frequency diagrams), including the nominal stress ranges $\Delta\sigma$ and corresponding cycle numbers n, are obtained from the nominal stress time series by the rainflow-counting method, as shown in Figure 10. The effective nominal stress range $\Delta\sigma_e$ is calculated by Equation (14):

$$\Delta\sigma_e = \left[\frac{1}{D_N}\cdot\frac{\sum_{i=1}^{k} n_i(\Delta\sigma_{\text{nom}-i})^{m_0}}{\sum_{i=1}^{k} n_i}\right]^{1/m_0} \tag{14}$$

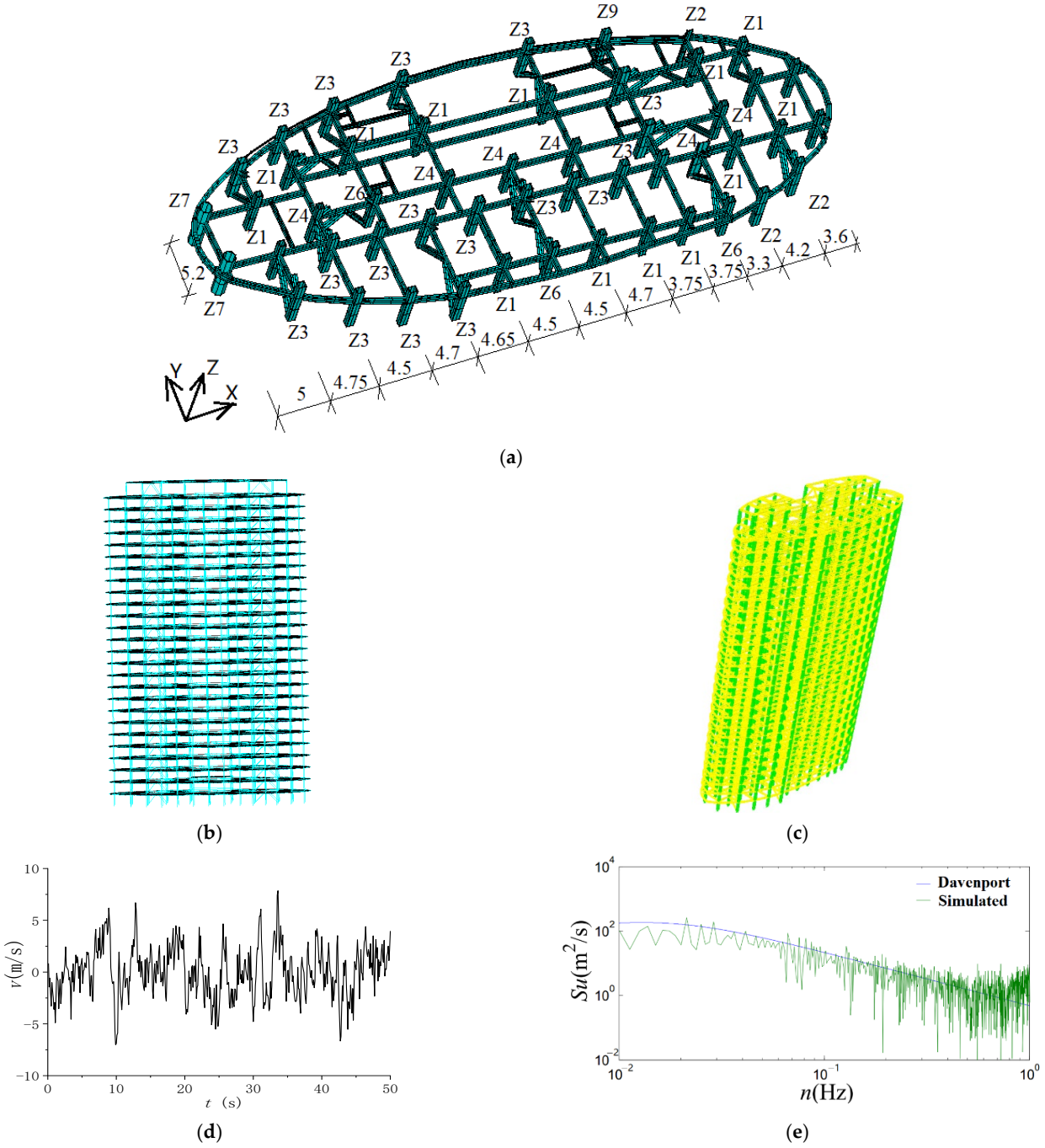

Figure 9. Summary of the building and the model. (**a**) Floor layout. (**b**) Finite element model in ANSYS. (**c**) Finite element model in ETABS. (**d**) Fluctuating wind speed time series. (**e**) Power spectrum comparison.

where $\Delta\sigma_{\mathrm{nom}-i}$ is the i-th nominal stress range causing fatigue damage in the cumulative frequency diagram; n_i is the cycle number under stress range $\Delta\sigma_{\mathrm{nom}-i}$; D_N is the specified Miner sum as 1. Based on the S-N curve of FAT36 suggested by IIW recommendation (IIW2259-15) for the nominal stress approach used in this connection, the fatigue damage within 50 s as D_t is calculated by Equation (15):

$$D_t = \frac{\Delta\sigma_e{}^{m_0} \sum_{i=1}^{k} n_i}{C_0} \tag{15}$$

where $C_0 = 4.143 \times 10^{13}$ and $m_0 = 5$ when $\Delta\sigma_{nom} \leq 21.1$ MPa (knee point of the S-N curve), while $C_0 = 9.331 \times 10^{10}$ and $m_0 = 3$ when $\Delta\sigma_{nom} > 21.1$ MPa [16]. The fatigue life T_0 (Unit: year) is calculated as shown in Equation (16):

$$T_0 = \frac{t_{50}}{D_t t_y} \tag{16}$$

where $t_{50} = 50$ s and t_y is the total time in one year, as 3.1536×10^7 s.

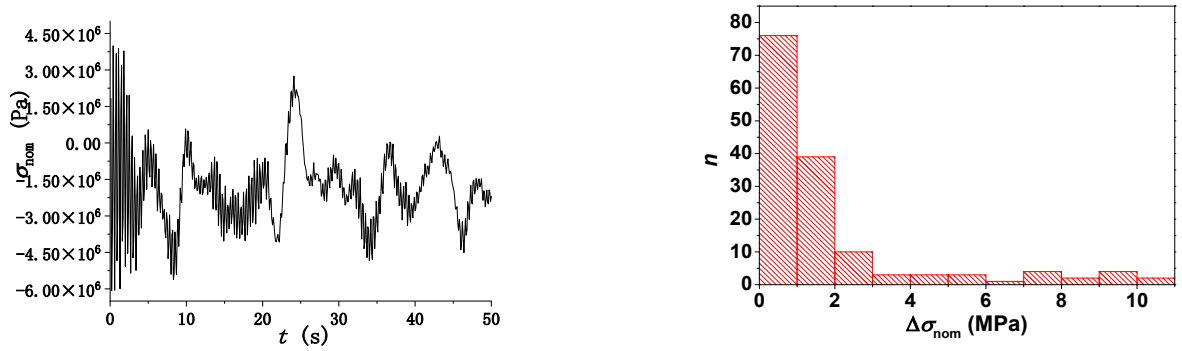

(**a**) (**b**)

Figure 10. Nominal stress information of Connection 5561. (**a**) Time-history of the nominal stress. (**b**) Nominal stress range spectrum.

The results of eight typical connections, as shown in Figure 9a, are listed in Table 5. It is found from the table that Connection 5725 is the critical connection with the greatest fatigue damage, and its fatigue life is 93 years, which tends to be dangerous during its service life of 100 years. Thus, fatigue damage mitigation using the VFD and the TMD is necessary and is discussed, respectively.

3.3. Structure with VFD Systems

According to the results of the time-history analysis in the previous section, the VFDs are installed at specific locations, as shown in Figure 9a, in two ways, haunched and braced, as shown in Figure 11, from the 1st floor to the 20th floor. The damping coefficient of the VFD is C = 500 kN·s/m and the damping exponent is $\alpha = 0.25$.

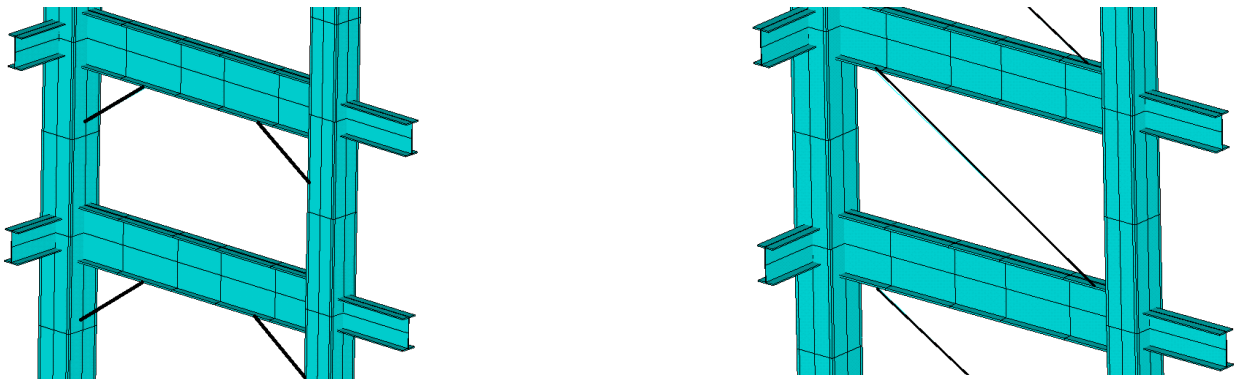

(**a**) (**b**)

Figure 11. Installation of the VFD. (**a**) Haunched. (**b**) Braced.

Table 5. Fatigue analysis results.

No.	$\sum_{i=1}^{k} n_i$	Connection without Damping Systems		Connection with VFD						Connection with TMD		
				Haunched			Braced					
		D_t	T_0 (Year)	D_t	$T_{e\text{-HVFD}}$ (Year)	k	D_t	$T_{e\text{-BVFD}}$ (Year)	k	D_t	$T_{e\text{-TMD}}$ (Year)	k
5561	138	1.08×10^{-8}	146	7.73×10^{-10}	2052	14.1	5.80×10^{-10}	2735	18.7	2.07×10^{-9}	765	5.2
5585	137	4.85×10^{-9}	326	3.75×10^{-10}	4226	13.0	3.13×10^{-10}	5062	15.5	1.06×10^{-9}	1489	4.6
5626	137	3.59×10^{-9}	441	3.04×10^{-9}	522	1.2	9.79×10^{-9}	162	0.4	1.09×10^{-9}	1459	3.3
5788	138	1.39×10^{-8}	113	2.05×10^{-9}	773	6.8	1.27×10^{-9}	1249	11.1	6.98×10^{-9}	227	2.0
5622	137	5.93×10^{-9}	267	5.27×10^{-9}	301	1.1	1.17×10^{-8}	135	0.5	1.78×10^{-9}	893	3.3
5659	138	1.55×10^{-8}	102	1.49×10^{-9}	1065	10.4	1.01×10^{-9}	1574	15.4	4.86×10^{-9}	326	3.2
5725	138	1.70×10^{-8}	93	2.33×10^{-9}	680	7.3	1.51×10^{-9}	1047	11.3	6.89×10^{-9}	230	2.5
5811	139	2.52×10^{-10}	6285	6.98×10^{-11}	22,718	3.6	3.02×10^{-11}	52,434	8.3	1.26×10^{-10}	12,535	2.0

The simulation of the VFDs is kept the same as that in Section 2.1. The time-history analysis and fatigue analysis are conducted and the results are shown in Figure 12a and Table 5, where $T_{e\text{-HVFD}}$ and $T_{e\text{-BVFD}}$ are the fatigue life of the connections in the structure with haunched VFDs and braced VFDs. Figure 12a indicates that the nominal stress is reduced dramatically with the equipment of either haunched VFDs or bracing VFDs. However, the reduction effect is better in the structure with braced VFD systems, with less cost than that with haunched VFD systems. It is found from Table 5 that the fatigue life is prolonged for most typical connections except two connections, 5626 and 5622. This may be explained by the situation that these two connections are just the position where the VFD is installed, so that the damping force output by the VFD leads to the increase in the local stress within these two connections during the energy dissipation and thus decrease the fatigue life. This phenomenon is completely different from that of a single beam-to-column connection in Section 2, whose local stress is also reduced, even when the VFD is installed within this connection itself.

The two typical connections of 5561 and 5621 with the braced VFD systems are selected to demonstrate the effect of different damping coefficients (500 kN·s/m, 600 kN·s/m, 700 kN·s/m, 800 kN·s/m and 900 kN·s/m) and damping exponents (0.25, 0.35, 0.45, 0.55 and 0.7) on fatigue damage mitigation. The results of a total of 25 parameter conditions are shown in Figure 12b,c, where a fatigue life ratio k is defined as Equation (4).

It is found from Figure 12b that the fatigue life is significantly prolonged for the connection without the direct installation of the VFD, such as Connection 5561, and the prolonged effect tends to decrease with the increase in the damping exponent. This stems from the fact that the velocity response of the structure is relatively small under wind and the VFD designed with a low damping exponent is more sensitive to the small velocity response and leads to a larger damping force output. However, with the increase in the damping exponent, the influence of the damping coefficient on the mitigation effect becomes less. For example, the increase in the damping coefficient can significantly improve the mitigation effect when the damping exponent is 0.25, while it has little effect on the mitigation effect when the damping exponent reaches 0.7. It indicates that a small damping exponent is enough to reach a satisfying mitigation effect for the structure under wind.

Meanwhile, the mitigation effect is relatively bad or even becomes negative due to the increase in the local stress in the connection with the direct installation of the VFD, such as Connection 5626. Under such circumstances, the damping exponent should be designed to be greater than 0.55 to obtain a positive mitigation effect, according to Figure 12c. However, the VFDs are directly installed in two locations, as shown in Figure 9a, involving only four connections, so that the parameter design of the other connections can still refer to that of Connection 5561.

Moreover, the VFD systems can also contribute well to the mitigation of structural responses at the same time, as shown in Figure 12d. It is found that the structural top displacement response decreases dramatically and instantly after the equipment of the VFD systems, which is due to the phenomenon found in Section 2 that the stress and the displacement results show similar and synchronous mitigation trends.

3.4. Structure with TMD Systems

The modal analysis of this structure, defined as Model C, is conducted before the design of the TMD systems and the results of the first three vibration modes are listed in Table 2, which are the first order of translation in the Y axis, the first order of translation in the X axis and the first order of rotation around the Z axis. The maximum displacement for the first vibration mode mainly excited by the wind loading is reached at the top of the structure, so that this location is optimal for the installation of the TMD. Therefore, TMD is installed at the top of the structure, as shown in Figure 13a, simulated using MASS21, and it is connected to the structure through COMBIN14.

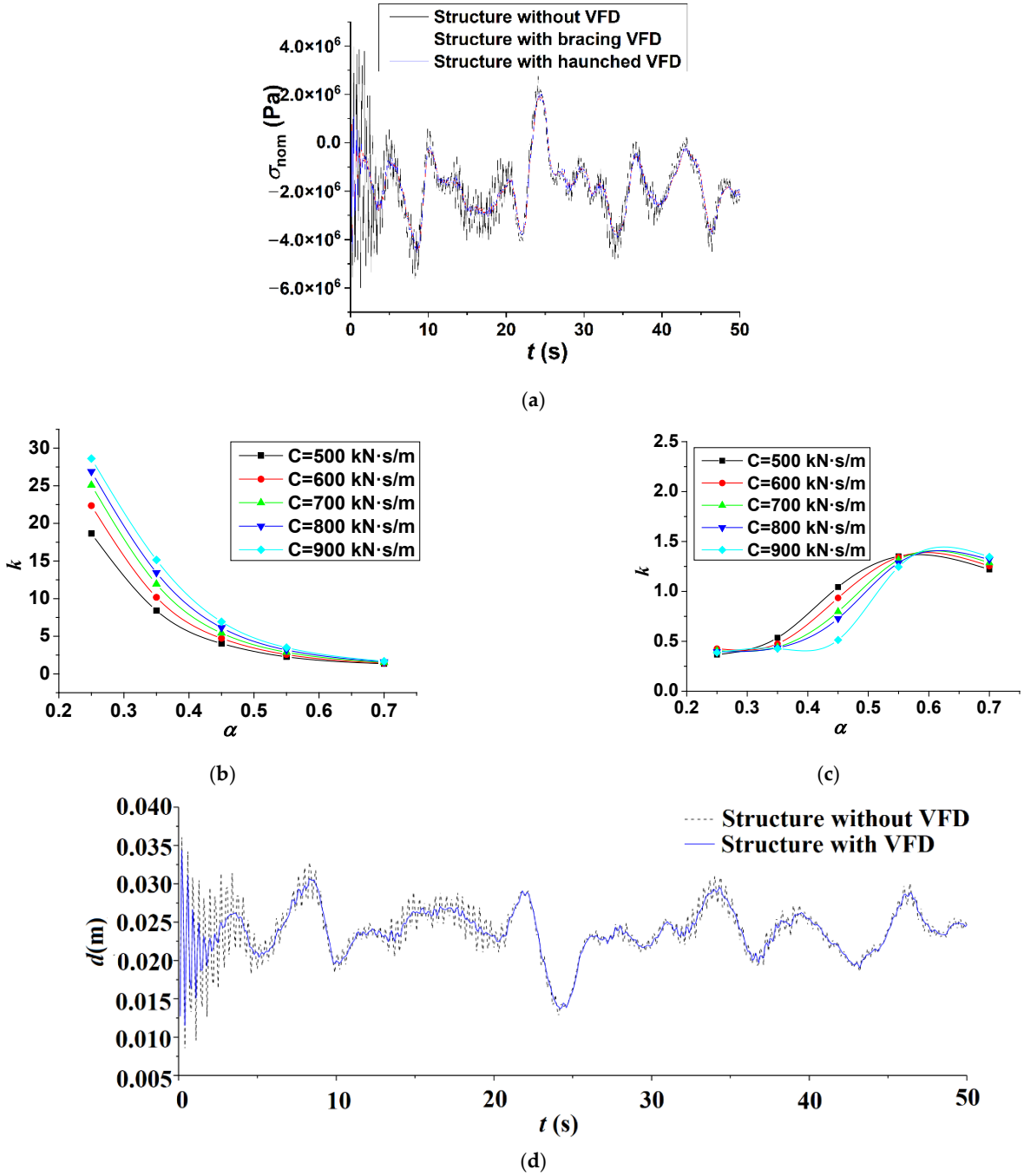

Figure 12. Fatigue mitigation effect of connections in structures with VFD systems. (**a**) Nominal stress time-history. (**b**) Parametric study of Connection 5561. (**c**) Parametric study of Connection 5626. (**d**) Time-history of structural top displacement response.

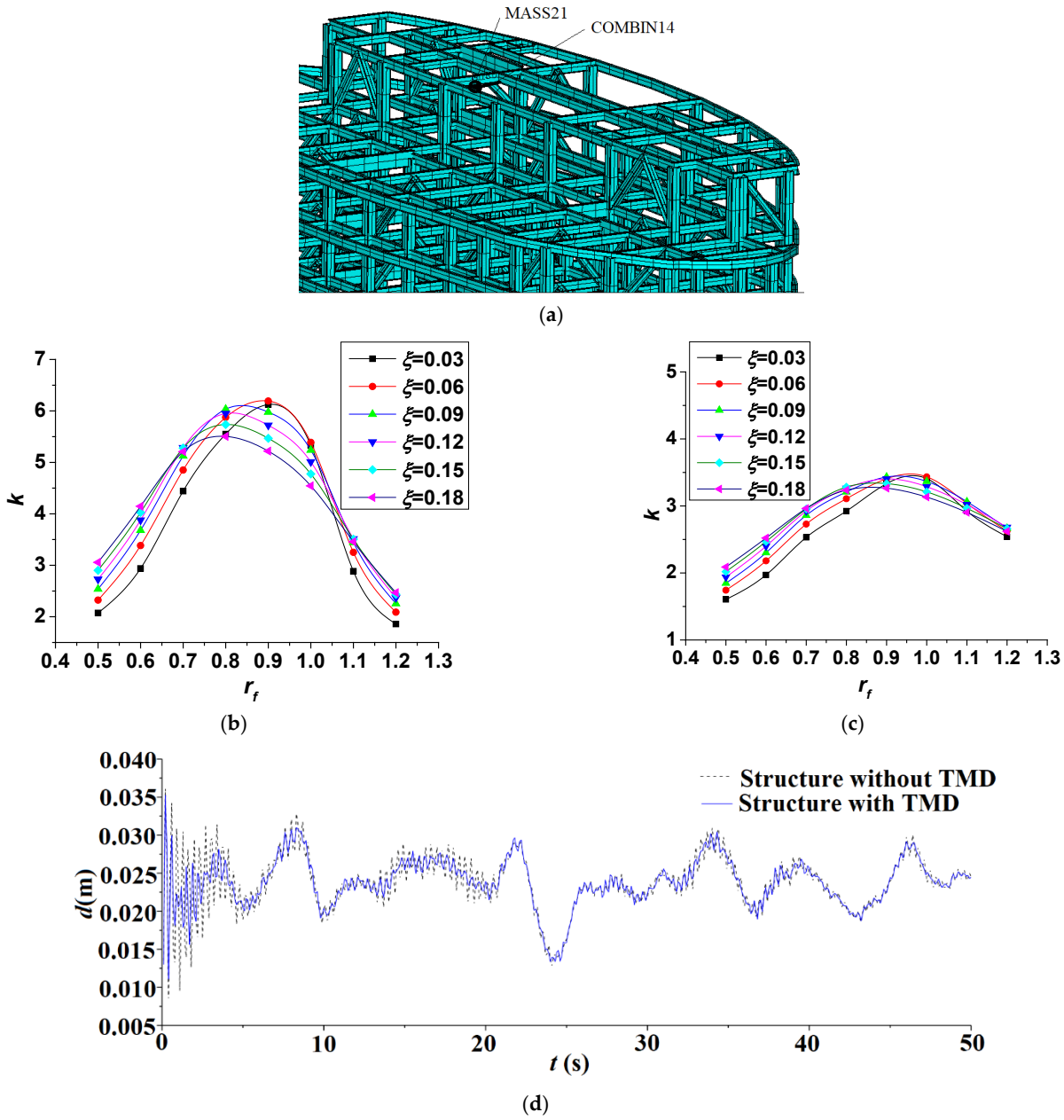

Figure 13. Fatigue mitigation effect of connections in structures with the TMD. (**a**) Installation of the TMD. (**b**) Parametric study of Connection 5561. (**c**) Parametric study of Connection 5626. (**d**) Time-history of structural top displacement response.

The mass ratio is set to be μ = 0.05 and the optimal parameters for the TMD under wind loading suggested by Den Hartog are calculated and listed in Table 2. After the time-history analysis and the fatigue analysis are both conducted, the fatigue life and ratio results are listed in Table 5. It is found from Table 5 that the fatigue damage mitigation using the TMD with generally smaller k values is not as effective as that using the VFDs on the same connection in the same structure, which agrees with the phenomenon in Section 2. Thus, it comes to the conclusion that the VFD is generally more effective in fatigue damage mitigation than the TMD for welded beam-to-column connections in steel high-rise buildings. Regarding the economic effect, the VFD is more economical and easier to install for the mitigation of a small amount of connections, while the TMD is more economical and easier to install for the mitigation of all the connections in a high-rise building.

To better demonstrate the effect of technical parameters on the mitigation results, the influence of different frequency ratios (r_f = 0.5, 0.6, 0.7, 0.8, 0.9, 1.0, 1.1, 1.2) and damping ratios (ξ = 0.03, 0.06, 0.09, 0.12, 0.15, 0.18) on the fatigue performance of two typical connections, Connection 5561 and 5626, is studied. The variation trend of the k value with both the two parameters is shown in Figure 13b,c.

It is found from Figure 13b,c that the frequency ratio has a greater impact on the fatigue life results, compared with the damping ratio. With the increase in the frequency ratio at the early stage, the fatigue life ratio tends to increase and it reaches the maximum value when the frequency ratio is generally between 0.9–1.0, which indicates the optimal mitigation effect and it agrees with the optimal frequency ratio of 0.952 calculated based on the theory proposed by Den Hartog. After that, the fatigue life ratio shows a decreasing trend when the frequency ratio continues to increase.

The effect of the damping ratio is much more complex. The fatigue life ratio increases with the damping ratio when the frequency ratio is less than about 0.8. However, it starts to decrease with the damping ratio when the frequency ratio is between 0.8 and 1.05. When the frequency ratio is finally greater than 1.05, the fatigue life ratio starts to increase again or keeps almost constant with the increase in the damping ratio. It also explains the reason why the damping ratio of the TMD only leads to the decrease in the mitigation effect under a frequency ratio of 0.98 for the single connection in Section 2.

Moreover, TMD systems also contribute well to the mitigation of structural displacement responses at the same time, as shown in Figure 13d. It is found from the figure that, after the equipment of the TMD system, the fluctuation of the structural top displacement response d decreases dramatically. In addition to that, based on the comparison of Figures 12d and 13d, it is obvious that the structural top displacement response starts to decrease from the first fluctuating peak in the structure with the VFD, while it starts to decrease from the second and the third fluctuating peak, which agrees with the phenomenon found for the single connection in Section 2 that the VFD starts to take effect almost instantly, while the TMD starts to take effect after one or two cycles.

4. Discussion

4.1. Optimization of Damper Positions

In the previous sections, the fatigue damage mitigation using VFD systems or TMD systems is discussed. It is obvious that the layout positions of the dampers definitely affect the mitigation effect. Since the layout of numerous VFDs is much more complex than a single TMD, the VFD systems are taken as an example and the optimization of their layout positions is discussed in this section.

In theory, the most economical and efficient layout plan is to place VFDs in a single optimum position for each floor and thus the single position layout is discussed. The VFD is placed in ten typical positions (C1–C10) from the 1st floor to the 20th floor, as shown in Figure 14a. The fatigue life and the ratio k results for some typical beam-to-column connections on the 11th floor are shown in Table 6. For a better comparison, the k value results for these connections are illustrated in Figure 14b, where the maximum relative displacement and maximum relative velocity between the two positions which connect the two ends of the potential dampers in the model without VFDs from C1 to C10 are also listed in the legend part of Figure 14b.

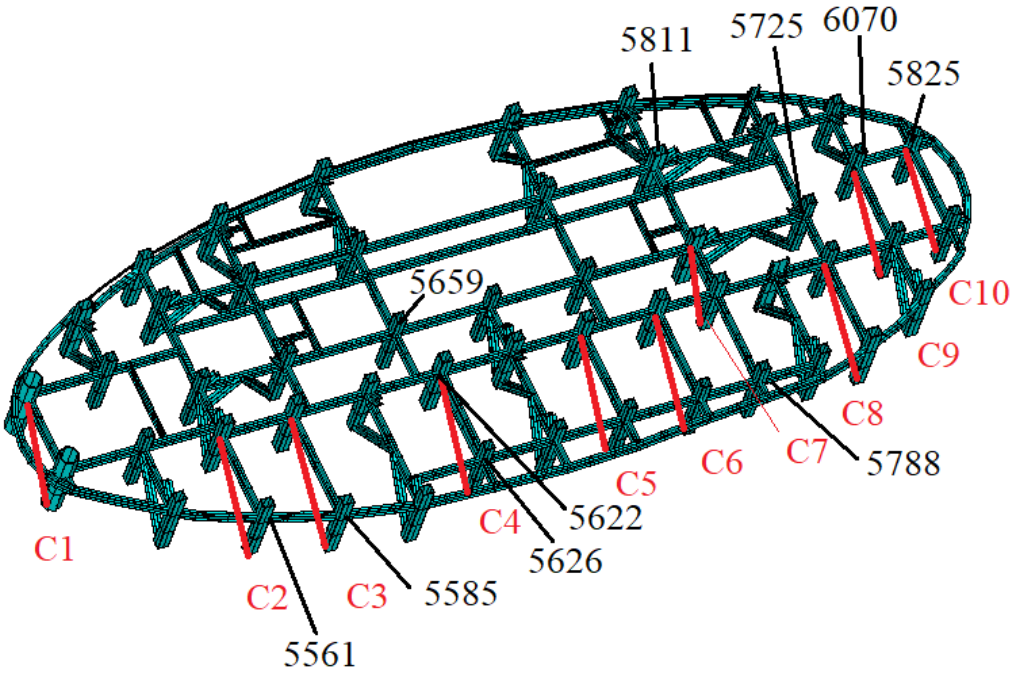
5811
5725
6070
5825
5659
C10
C9
C8
C7
C6
C5
C4
C3
C2
C1
5788
5622
5626
5585
5561

(a)

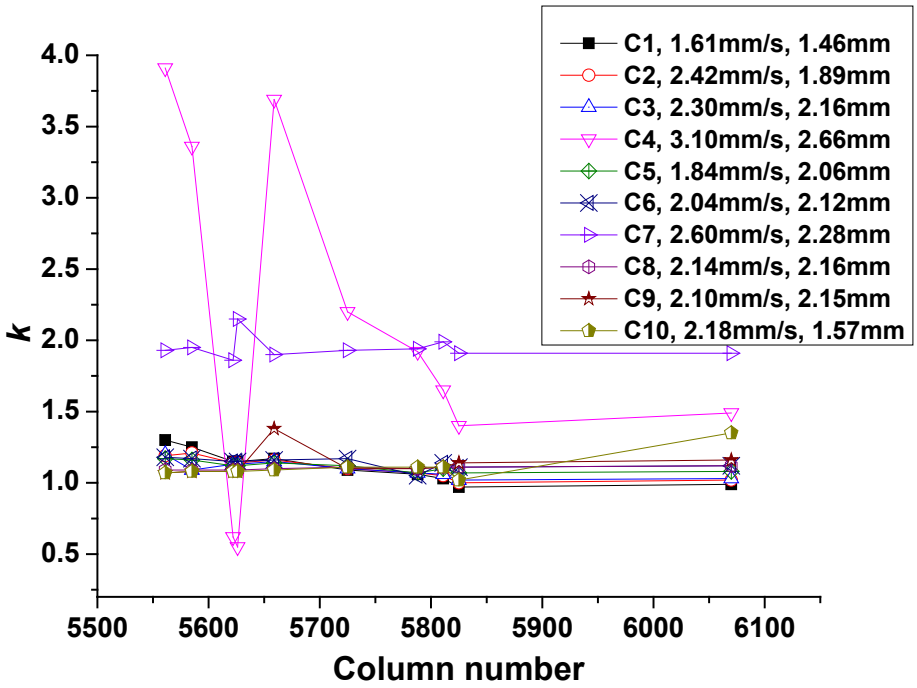
C1, 1.61mm/s, 1.46mm
C2, 2.42mm/s, 1.89mm
C3, 2.30mm/s, 2.16mm
C4, 3.10mm/s, 2.66mm
C5, 1.84mm/s, 2.06mm
C6, 2.04mm/s, 2.12mm
C7, 2.60mm/s, 2.28mm
C8, 2.14mm/s, 2.16mm
C9, 2.10mm/s, 2.15mm
C10, 2.18mm/s, 1.57mm
k
4.0
3.5
3.0
2.5
2.0
1.5
1.0
0.5
5500
5600
5700
5800
5900
6000
6100
Column number

(b)

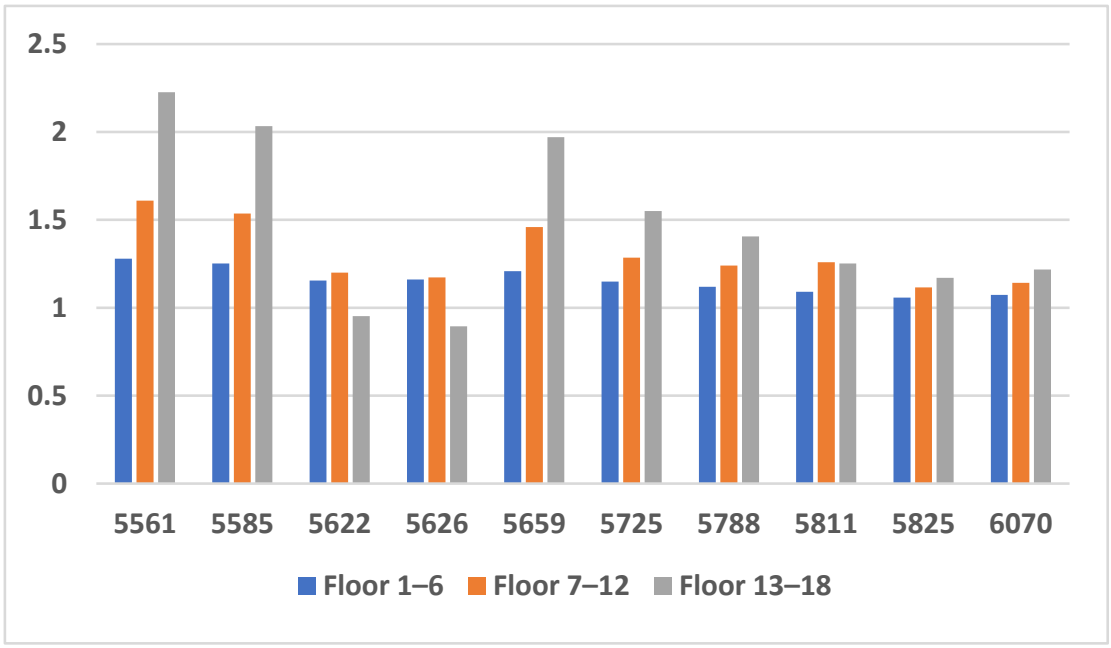

(**c**)

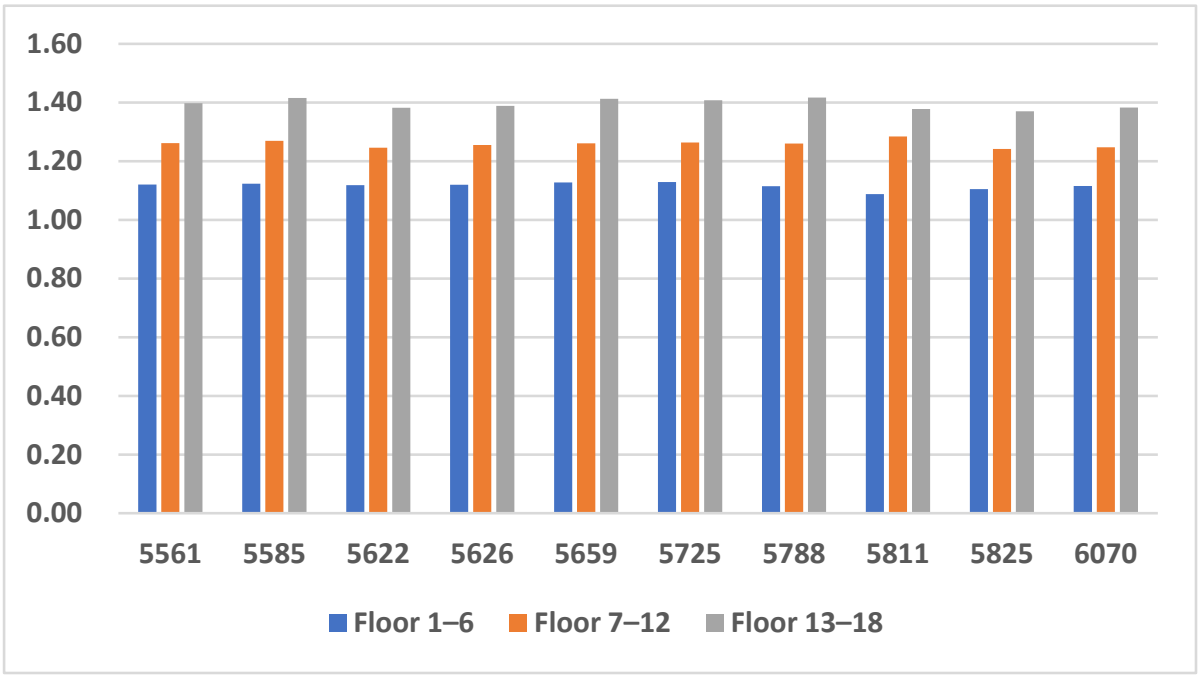

(**d**)

Figure 14. Layout of VFDs and results of *k* values in connections. (**a**) Layout plan of VFDs from C1 to C10. (**b**) Results of *k* values in different connections on the 11th floor. (**c**) Results of *k* values in connections with VFDs being installed in C4 on different floors. (**d**) Results of *k* values in connections with VFDs being installed in C4 on different floors.

Table 6. Results of fatigue life and k values in connections with VFDs in positions from C1 to C10.

VFD Positions	Fatigue Life	5561	5585	5622	5626	5659	5725	5788	5811	5825	6070
Without VFD	T_0 (Year)	161	353	325	543	100	95	257	3.24×10^8	186	230
C1	T_c (Year)	209	441	373	625	117	103	271	3.33×10^8	181	230
	k	1.30	1.25	1.15	1.15	1.17	1.09	1.06	1.03	0.97	0.99
C2	T_c (Year)	192	427	371	621	116	104	274	3.40×10^8	186	230
	k	1.19	1.21	1.14	1.14	1.16	1.10	1.07	1.05	1.00	1.02
C3	T_c (Year)	194	386	367	615	115	104	276	3.43×10^8	189	240
	k	1.20	1.09	1.13	1.13	1.15	1.10	1.07	1.06	1.02	1.03
C4	T_c (Year)	630	1187	202	300	369	209	494	5.34×10^8	260	340
	k	3.91	3.36	0.62	0.55	3.69	2.20	1.92	1.65	1.40	1.49
C5	T_c (Year)	188	409	363	608	114	107	274	3.56×10^8	199	250
	k	1.17	1.16	1.12	1.12	1.14	1.12	1.07	1.10	1.07	1.08
C6	T_c (Year)	190	415	374	626	116	111	270	3.69×10^8	207	260
	k	1.18	1.17	1.15	1.15	1.16	1.17	1.05	1.14	1.11	1.12
C7	T_c (Year)	311	689	605	1168	190	183	498	6.44×10^8	356	440
	k	1.93	1.95	1.86	2.15	1.90	1.93	1.94	1.99	1.91	1.91
C8	T_c (Year)	176	386	356	594	110	105	284	3.59×10^8	207	260
	k	1.09	1.09	1.09	1.09	1.10	1.11	1.10	1.11	1.11	1.12
C9	T_c (Year)	173	380	352	588	138	105	283	3.60×10^8	212	270
	k	1.07	1.08	1.08	1.08	1.38	1.10	1.10	1.11	1.14	1.16
C10	T_c (Year)	172	380	352	588	109	105	284	3.61×10^8	189	310
	k	1.07	1.08	1.08	1.08	1.09	1.11	1.11	1.11	1.02	1.35

It is found from the table and the figure that the fatigue ratio k mainly depends on two things. The first and the most important one is the relative displacement and relative velocity between the two positions which connect the two ends of the potential dampers in the model without VFDs. It is found that the k value tends to increase in the positions simultaneously with large maximum relative displacement and relative velocity. It leads to the fact that, when the dampers are installed in the positions of C4 and C7 with large relative displacement and relative velocity, the k value can even reach a rather large value. Meanwhile, when the dampers are installed in other positions, such as C2 and C3, the relative displacement is relatively small, though they have a large maximum relative velocity, which leads to a smaller k value compared with C4 and C7. It indicates that the relative displacement and relative velocity between the two positions which connect the two ends of the potential dampers determine the k value simultaneously. It is rather easy to understand, since the fatigue mitigation comes from the working of the dampers and the working efficiency is strongly related to the relative displacement and relative velocity between the two ends. Meanwhile, relative displacement and relative velocity are rather close to each other in these connections when the dampers are installed in positions other than C4 and C7, which leads to similar k values.

The second thing that needs to be mentioned is the distance from the targeted beam-to-column connection to the VFD installation positions. If the VFD is installed near to the targeted connection, a larger k value is probably obtained in these connections, such as Connection 5561 with C1 position, Connection 5561 and 5585 with C2 and C3 positions, Connection 5659 with C4 position, Connection 5788 and 5811 with C7 position, etc. Meanwhile, the installation of the VFD directly at the targeted connection usually also leads to a relatively large, though sometimes not optimum, k value, such as Connection 5561 with C2 position, Connection 5585 with C3 position, Connection 6070 with C9 position, etc. However, there is one special case where a k value smaller than 1 is found in both

Connection 5622 and 5626 when dampers are installed in the position of C4, just between the two connections, which indicates a negative fatigue damage mitigation effect. This special case is discussed in Section 4.2.

In addition to the above analysis, the layout of VFDs on different floors is also discussed. The VFDs are installed in the positions of C4 and C7 on floors from 1 to 6 (low floors), from 7 to 12 (middle floors) and from 13 to 18 (high floors). The results for C4 and C7 positions are, respectively, listed in Figure 14c,d. It is found from the figure that the k value tends to increase when the VFDs are placed on high floors in almost all the connections, although the targeted connections are all on the 10th floor, as a middle floor. It means that the VFDs should be placed on higher floors instead of lower floors or middle floors, even if they contain the targeted connection.

Based on the above analysis, it is concluded that, for the sake of a better fatigue damage mitigation effect in a targeted beam-to-column connection, the optimized VFD layout plan should be that VFDs are placed between the two connections with large relative displacement and relative velocity on higher floors to increase their working efficiency and, moreover, these two connections with VFDs should be near to the targeted connection.

4.2. Negative Mitigation Effect

It has been pointed out that Connection 5622 and Connection 5626 both show negative fatigue damage mitigation effect, where the k values are smaller than 1. To better understand this phenomenon, all the connections directly with the VFDs in the positions from C1 to C10 are illustrated in Figure 15 and the k value results of these connections are listed in Table 7. In the table, the VFDs are placed between the Connection i and Connection j. Connection i is the connection on the south side, such as 5271, 5561, 5585, etc. Connection j means the connection on the north side, such as 5286, 5317, 5333, etc.

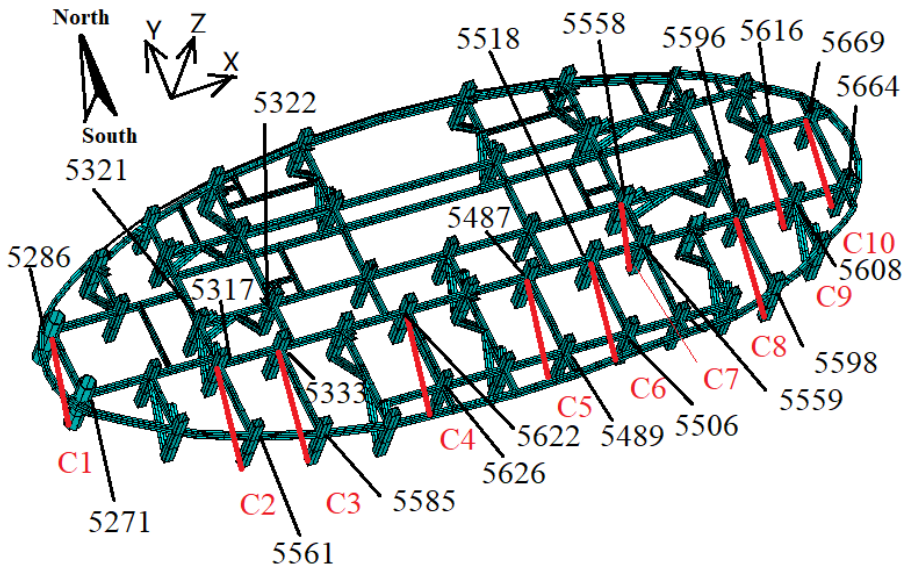

Figure 15. Layout of two end connections with VFDs in positions from C1 to C10.

It is found from the table that the connections directly equipped with VFDs in the positions of C4, C5 and C6 show a negative fatigue damage mitigation effect, while other connections all show a positive fatigue damage effect. It means that the direct equipment does not always lead to a negative mitigation effect. It is found from Figure 15 that Connection j with the damping positions of C4, C5 and C6 are all without direct lateral support of beams from the north side in the Y-axis direction, such as Connections 5622, 5487 and 5518, which means that the lateral support force exerted on these three connections in the Y-axis is generally low and thus may result in serious stress concentration within these connections when the VFD is installed. On the contrary, Connection j of most other connections are all supported by lateral beams directly from the north side in the Y-axis to

provide enough lateral force and thus may avoid serious stress concentration within these connections. It is worth noting that Connection *j* with the position of C3 (Connection 5333), which is not directly supported by lateral beams, still shows a positive mitigation effect. This may stem from the fact that the bracing between Connection 5321 and Connection 5322 and that between Connection 5321 and Connection 5317 near to this connection provides additional lateral support and the support force is transmitted to Connection 5333, which thus may avoid serious stress concentration. On the contrary, Connections 5622, 5487 and 5518 do not have such a source of lateral support force. Therefore, it is concluded that the negative fatigue damage mitigation mainly stems from an insufficient lateral support force, so that the direct installation of VFDs may result in a negative fatigue damage mitigation effect in the connections with limited lateral support.

Table 7. Results of fatigue life and *k* values in the two end connections with VFDs in positions from C1 to C10.

			C1	**C2**	**C3**	**C4**	**C5**	**C6**	**C7**	**C8**	**C9**	**C10**
Model without VFD	Connection *i*	T_0 (Year)	136	161	353	543	319	190	258	911	210	206
	Connection *j*	T_0 (Year)	136	130	321	325	208	130	181	1015	230	186
Model with VFD	Connection *i*	T_c (Year)	181	192	386	300	203	90	270	1027	210	213
	Connection *j*	T_c (Year)	179	156	342	202	203	60	189	1136	270	189
	Connection *i*	*k*	1.33	1.19	1.09	0.55	0.64	0.46	1.05	1.13	1.00	1.03
	Connection *j*	*k*	1.31	1.20	1.06	0.62	0.97	0.50	1.04	1.12	1.16	1.01

5. Conclusions

(1) The VFD and the TMD systems are both effective in local fatigue damage mitigation, along with structural displacement mitigation, for both a single connection under constant amplitude cyclic loading and multi-connections in a high-rise building under stochastic wind, while the mitigation effect decreases in the low-cycle fatigue condition compared with the high-cycle fatigue condition; therefore, these two passive control systems both have promising usability in fatigue damage mitigation of welded beam-to-column connections in steel high-rise buildings.

(2) The VFD generally has a better mitigation effect than the TMD and it starts to take effect instantly with external loading and is equally effective in connections and structures with almost all ranges of natural frequencies, but it causes a phase difference in the structural responses, including stress and displacement. On the contrary, the TMD starts to take effect after a few cycles and is more effective in connections and structures with a lower natural frequency, and it does not change the phase of the structural responses. Regarding the economic effect, the VFD is more economical and easier to install for the mitigation of one or several connections, while the TMD is more economical and easier to install for the mitigation of all the connections in a high-rise building.

(3) The VFD system should be designed with a small damping exponent and a large damping coefficient in the braced installation form, while the TMD system can be designed according to the optimal parameters, so that the two systems are more optimal to both the local stress and the structural displacement, since the two indexes are found to show similar and synchronous mitigation trends and thus the VFD and the TMD can be designed based on either the local stress or the structural displacement.

(4) For the sake of a better fatigue damage mitigation effect in a targeted beam-to-column connection, the optimized VFD layout plan is that VFDs are placed between the two connections with large relative displacement and relative velocity on higher floors to increase their working efficiency; moreover, these two connections with VFDs should be near to the targeted connection.

(5) The negative fatigue damage mitigation mainly stems from an insufficient lateral support force so that the direct installation of VFDs may result in a negative fatigue damage mitigation effect in the connections with limited lateral support.

Author Contributions: Conceptualization, Z.F. and J.Z.; methodology, A.L.; software, F.Y.; validation, Z.F., J.Z. and F.Y.; formal analysis, Z.F. and J.Z.; investigation, Z.F. and J.Z.; resources, Z.F.; data curation, Z.F. and J.Z.; writing—original draft preparation, Z.F. and J.Z.; writing—review and editing, Z.F.; visualization, F.Y.; supervision, A.L.; project administration, A.L.; funding acquisition, Z.F. and A.L. All authors have read and agreed to the published version of the manuscript.

Funding: This research was supported by the National Natural Science Foundation of China (No.52008202, No.51978154 and No.52108108), the Distinguished Young Scientists of Jiangsu Province (No. BK20190013), the Natural Science Foundation of Jiangsu Province in China (No. BK20191016 and No. BK20191013) and the Beijing Postdoctoral Research Foundation (2021-zz-105).

Institutional Review Board Statement: Not applicable.

Informed Consent Statement: Not applicable.

Data Availability Statement: Due to the nature of this research, participants of this study did not agree for their data to be shared publicly, so supporting data is not available.

Conflicts of Interest: The authors declare no conflict of interest.

References

1. Plumier, A.; Agatino, M.R.; Castellani, A.; Castiglioni, C.A.; Chesi, C. Resistance of steel connections to low-cycle fatigue. In Proceedings of the 11th European Conference on Earthquake Engineering, Paris, France, 6–11 September 1998.
2. Soong, T.T.; Dargush, G.F. *Passive Energy Dissipation Systems in Structural Engineering*; John Wiley & Sons: New York, NY, USA, 1998.
3. Janbazi, R.H.; Tabeshpour, M.R. Spectral fatigue analysis of jacket platform under wave load equipped with viscous damper. *J. Mar. Sci. Technol.* **2019**, *24*, 855–870. [CrossRef]
4. Allen, C.K.; Goupee, A.J.; Viselli, A.M. A computationally-efficient frequency domain model of a floating wind turbine with hull-based tuned mass damper elements. In Proceedings of the 31st International Ocean and Polar Engineering Conference, Rhodes, Greece, 20–25 June 2021.
5. Repetto, M.P.; Solari, G. Wind-induced fatigue collapse of real slender structures. *Eng. Struct.* **2010**, *32*, 3888–3898. [CrossRef]
6. Repetto, M.P.; Solari, G. Dynamic alongwind fatigue of slender vertical structures. *Eng. Struct.* **2001**, *23*, 1622–1633. [CrossRef]
7. Bhowmik, B.; Tripura, T.; Hazra, B.; Pakrashi, V. Real time structural mod25al identification using recursive canonical correlation analysis and application towards online structural damage detection. *J. Sound Vib.* **2020**, *468*, 115101. [CrossRef]
8. Bhowmik, B.; Tripura, T.; Hazra, B.; Pakrashi, V. First-order eigen-perturbation techniques for real-time damage detection of vibrating systems: Theory and applications. *Appl. Mech. Rev.* **2019**, *71*, 060801. [CrossRef]
9. Prawin, J. Real-time reference-free breathing crack identification using ambient vibration data. *Struct. Control. Health Monit.* **2022**, *29*, e2903. [CrossRef]
10. Palmeri, A.; Ricciardelli, F. Fatigue analyses of buildings with viscoelastic dampers. *J. Wind Eng. Ind. Aerodynamics.* **2006**, *94*, 377–395. [CrossRef]
11. Golafshani, A.A.; Gholizad, A. Passive vibration control for fatigue damage mitigation in steel jacket platforms. *Int. J. Eng.* **2008**, *21*, 313–324.
12. Ambrosio, P.; Cazzulani, G.; Resta, F.; Ripamonti, F. An optimal vibration control logic for minimising fatigue damage in flexible structures. *J. Sound Vib.* **2014**, *333*, 1269–1280. [CrossRef]
13. Ripamonti, F.; Cazzulani, G.; Cinquemani, S.; Resta, F.; Torti, A. Adaptive active vibration control to improve the fatigue life of a carbon-epoxy smart structure. In *Active and Passive Smart Structures and Integrated Systems, Proceedings of the SPIE Smart Structures and Materials + Nondestructive Evaluation and Health Monitoring, San Diego, CA, USA, 8–12 March 2015*; SPIE: Bellingham, WA, USA, 2015; pp. 732–740.
14. Andersson, A.; O'Connor, A.; Karoumi, R. Passive and adaptive damping systems for vibration mitigation and increased fatigue service life of a tied arch railway bridge. *Comput.-Aided Civ. Infrastruct. Eng.* **2015**, *30*, 748–757. [CrossRef]
15. Radaj, D.; Sonsino, C.M.; Flade, D. Prediction of service fatigue strength of a welded tubular joint on the basis of the notch strain approach. *Int. J. Fatigue* **1998**, *20*, 471–480. [CrossRef]
16. Hobbacher, A. *Recommendations for Fatigue Design of Welded Joints and Components*; Springer: Dordrecht, The Netherlands, 2015.
17. Fang, Z.; Li, A.; Li, W.; Shen, S. Wind-induced fatigue analysis of high-rise steel structures using equivalent structural stress method. *Appl. Sci.* **2017**, *7*, 71. [CrossRef]
18. Fang, Z.; Li, A.; Ding, Y.; Li, W. Wind-induced fatigue assessment of welded connections in steel tall buildings using the theory of critical distances. *Eur. J. Environ. Civ. Eng.* **2020**, *24*, 1180–1205. [CrossRef]

19. Fang, Z.; Li, A.; Ding, Y.; Shen, S. Three-dimensional surface fatigue crack growth life assessment model of steel welded joints and structures. *Adv. Struct. Eng.* **2022**, *25*, 1776–1791. [CrossRef]
20. Den Hartog, J.P. *Mechanical Vibrations*; McGraw-Hill Book Company: New York, NY, USA, 1956.
21. Den Hartog, J.P. *Mechanical Vibrations*; Dover Publications: New York, NY, USA, 1985.
22. Kelly, S.G.; Kudari, S. *Mechanical Vibrations*; Tata McGraw-Hill Publishing Co., Ltd.: New Delhi, India, 2009.
23. Socie, D.F. Fatigue-life prediction using local stress-strain concepts. *Exp. Mech.* **1977**, *17*, 50–56. [CrossRef]
24. Ubertini, F.; Giuliano, F. Computer simulation of stochastic wind velocity fields for structural response analysis: Comparisons and applications. *Adv. Civ. Eng.* **2010**, *83*, 441–456. [CrossRef]